

# DeeP-LCC: Data-Enabled Predictive Leading Cruise Control in Mixed Traffic Flow

Jiawei Wang<sup>1</sup>, Graduate Student Member, IEEE, Yang Zheng<sup>2</sup>, Member, IEEE, Keqiang Li<sup>1</sup>, and Qing Xu

**Abstract**—For the control of connected and autonomous vehicles (CAVs), most existing methods focus on model-based strategies. They require explicit knowledge of car-following dynamics of human-driven vehicles that are nontrivial to identify accurately. In this article, instead of relying on a parametric car-following model, we introduce a data-driven nonparametric strategy, called Data-Enabled Predictive Leading Cruise Control (DeeP-LCC), to achieve safe and optimal control of CAVs in mixed traffic. We first utilize Willems’ fundamental lemma to obtain a data-centric representation of mixed traffic behavior. This is justified by rigorous analysis on controllability and observability properties of mixed traffic. We then employ a receding horizon strategy to solve a finite-horizon optimal control problem at each time step, in which input–output constraints are incorporated for collision-free guarantees. Numerical experiments validate the performance of DeeP-LCC compared to a standard predictive controller that requires an accurate model. Multiple nonlinear traffic simulations further confirm its great potential on improving traffic efficiency, driving safety, and fuel economy.

**Index Terms**—Connected vehicles, data-driven control, mixed traffic, model predictive control.

## I. INTRODUCTION

WIRELESS communication technologies, e.g., vehicle-to-vehicle (V2V) or vehicle-to-infrastructure (V2I), have provided new opportunities for advanced vehicle control and enhanced traffic mobility [1]. With access to beyond-the-sight information and edge/cloud computing resources, individual vehicles are capable to make sophisticated decisions and even cooperate with each other to achieve system-wide traffic optimization. One typical technology is Cooperative Adaptive Cruise Control (CACC), which organizes a series of connected and autonomous vehicles (CAVs) into a platoon and applies cooperative control strategies to achieve smaller spacing, better fuel economy, and smoother traffic flow [2], [3], [4].

Manuscript received 11 January 2023; accepted 9 June 2023. Date of publication 4 July 2023; date of current version 23 October 2023. The work of Jiawei Wang, Keqiang Li, and Qing Xu was supported in part by the National Key Research and Development Program of China under Grant 2018YFE0204302, in part by the National Natural Science Foundation of China under Grant 52072212, and in part by the Tsinghua University–Didi Joint Research Center for Future Mobility. Recommended by Associate Editor E. Hellström. (Corresponding authors: Yang Zheng; Qing Xu.)

Jiawei Wang, Keqiang Li, and Qing Xu are with the School of Vehicle and Mobility, Tsinghua University, Beijing 100084, China (e-mail: wang-jw18@mails.tsinghua.edu.cn; likq@tsinghua.edu.cn; qingxu@tsinghua.edu.cn).

Yang Zheng is with the Department of Electrical and Computer Engineering, University of California at San Diego, La Jolla, CA 92093 USA (e-mail: zhengy@eng.ucsd.edu).

Color versions of one or more figures in this article are available at <https://doi.org/10.1109/TCST.2023.3288636>.

Digital Object Identifier 10.1109/TCST.2023.3288636

In practice, CACC or platooning requires all the involved vehicles to have autonomous capabilities. Considering the gradual deployment of CAVs, the transition phase of mixed traffic with the coexistence of human-driven vehicles (HDVs) and CAVs may last for decades [5], [6], [7]. HDVs, connected to V2V/V2I communication but still controlled by human drivers, will still be the majority on public roads in the near future. Without explicitly considering surrounding HDVs’ behavior, CAVs at a low penetration rate may only bring negligible benefits on traffic performance [8], [9]. One extension of CACC to mixed traffic is Connected Cruise Control (CCC) [10], in which one single CAV at the tail makes its control decisions by exploiting the information of multiple HDVs ahead. Another recent extension is Leading Cruise Control (LCC) that incorporates the motion of HDVs ahead and behind [11].

Existing CAV control, e.g., CACC and CCC, mainly takes local-level performance into consideration—the CAVs aim to improve their own driving performance. Considering the interactions among surrounding vehicles, a recent concept of Lagrangian control in mixed traffic aims to focus on system-level performance of the entire traffic flow by utilizing CAVs as mobile actuators [5], [6], [12]. In particular, the real-world experiment in [5] demonstrates the potential of one single CAV in stabilizing a ring-road mixed traffic system. This has been subsequently validated from rigorous theoretical analysis [6], [13] and large-scale traffic simulations [12], [14]. These results focus on a closed circular road setup [15]. The recent notion of LCC [11] focuses on general open straight road scenarios and has provided further insight into CAV control in mixed traffic: one single CAV can not only adapt to the downstream traffic flow consisting of its preceding HDVs (as a follower) but also improve the upstream traffic performance by actively leading the motion of its following HDVs (as a leader). This explicit consideration of a CAV as both a leader and a follower greatly enhances its capability in smoothing mixed traffic flow, as demonstrated both empirically and theoretically in [11]. One challenge is to design LCC strategies with safety guarantees in smoothing traffic flow when the traffic model is not known.

## A. Model-Based and Model-Free Control of CAVs

Mixed traffic is a complex human-in-the-loop cyber-physical system, in which HDVs are controlled by human drivers with uncertain and stochastic behaviors. Most existing studies exploit microscopic car-following models and design model-based control strategies for CAVs, such as linear

quadratic control [6], [16], structured optimal control [13],  $\mathcal{H}_\infty$  control [17], and model predictive control [18]. In practice, however, human car-following behaviors are complex and nonlinear, which are nontrivial to identify accurately. Model-free and data-driven methods, bypassing model identifications, have recently received increasing attention [19], [20]. For example, reinforcement learning [12], [14] and adaptive dynamic programming [21], [22] have been recently utilized for mixed traffic control. Instead of relying on explicit dynamics of HDVs, these methods utilize online and/or offline driving data of HDVs to learn CAVs' control strategies. However, these methods typically bring a heavy computation burden and are sample inefficient. Safety is a critical aspect for CAV control in practical deployment, but this has not been well addressed in the existing studies [12], [14], [21], [22]. Indeed, it remains challenging to include constraints to achieve safety guarantees for these model-free and data-driven methods [19].

On the other hand, model predictive control (MPC) has been widely recognized as a primary tool to address control problems with constraints [18], [23]. Recent advancements in data-driven MPC have further provided techniques toward safe learning-based control using measurable data [24], [25], [26]. One promising method is the data Enabled predictive control (DeePC) [26] that is able to achieve safe and optimal control for unknown systems using input-output measurements. Rather than identifying a parametric system model, DeePC relies on Willems' fundamental lemma [27] to directly learn the system behavior and predict future trajectories. In particular, DeePC allows one to incorporate input-output constraints to ensure safety. It has been shown theoretically that DeePC is equivalent to sequential system identification and MPC for deterministic linear time-invariant (LTI) systems [26], [28] and empirically that DeePC could achieve comparable control performance with respect to MPC with accurate model knowledge for stochastic and nonlinear systems [29], [30]. Recently, practical applications have been seen in quadcopter systems [31], power grids [32], and electric motor drives [33].

To the best of our knowledge, data-driven MPC methods, particularly the recent DeePC method, have not been discussed for mixed traffic control. Due to distinct and complex dynamical properties of mixed traffic systems, the aforementioned results [26], [32], [33] are not directly applicable.

## B. Contributions

In this article, we focus on the recent LCC framework [11] and design safe and optimal control strategies for CAVs to smooth mixed traffic flow. Our method requires no prior knowledge of HDVs' car-following dynamics. In particular, we introduce a Data-Enabled Predictive Leading Cruise Control (DeeP-LCC) strategy, in which the CAVs utilize measurable driving data for controller design with collision-free guarantees. Some preliminary results were presented in [34]. Our contributions of this work are given as follows.

We first establish a linearized state-space model for a general mixed traffic system with multiple CAVs and HDVs under the LCC framework. We directly use measurable driving

data as system output since the HDVs' equilibrium spacing is typically not measurable. This issue of unknown equilibrium spacing has been neglected in many recent studies on mixed traffic [13], [16], [21], [22], [24], [35]. We further show that the linearized mixed traffic system is not controllable (except the case when the first vehicle is a CAV) but is stabilizable and observable. These results are the foundations of our adaptation of DeePC [26] for mixed traffic control.

We then propose a DeeP-LCC method for CAV control, which directly utilizes HDVs' trajectory data and bypasses an explicit identification of a parametric car-following model. The standard DeePC requires the underlying system to be controllable [26], [27] and thus cannot be directly applied to mixed traffic. To resolve this, we introduce an external input signal to record the data of the head vehicle, i.e., the first vehicle at the beginning of the mixed traffic system. Together with CAVs' control input, this contributes to system controllability. Our DeeP-LCC formulation incorporates spacing constraints on the driving behavior and thus provides safety guarantees for CAVs when feasible. Furthermore, our DeeP-LCC is directly applicable to nonlinear and nondeterministic traffic systems.

We finally carry out multiple traffic simulations to validate the performance of DeeP-LCC. DeeP-LCC achieves comparable performance in nonlinear and nondeterministic cases with respect to a standard MPC based on an accurate linearized model. We also design an urban/highway driving scenario motivated by the New European Driving Cycle (NEDC) and an emergence braking scenario. Numerical results confirm the benefits of DeeP-LCC in improving driving safety, fuel economy, and traffic smoothness. In particular, DeeP-LCC reduces up to 24.69% fuel consumption with safety guarantees in the braking scenario at a CAV penetration rate of 25% compared with the case of all HDVs.

## C. Article's Organization and Notation

The rest of this article is organized as follows. Section II introduces the modeling for the mixed traffic system, and Section III presents the controllability and observability analysis. This is followed by a brief review of the standard DeePC in Section IV. We present DeeP-LCC in Section V. Traffic simulations are discussed in Section VI. Section VII concludes this article. Some auxiliary proofs and implementation details are included in the Appendix.

**Notations:** We denote  $\mathbb{N}$  as the set of natural numbers,  $\mathbf{0}_n$  as a zero vector of size  $n$ , and  $\mathbf{0}_{m \times n}$  as a zero matrix of size  $m \times n$ . For a vector  $a$  and a positive definite matrix  $X$ ,  $\|a\|_X^2$  denotes the quadratic form  $a^\top X a$ . Given a collection of vectors  $a_1, a_2, \dots, a_m$ , we denote  $\text{col}(a_1, a_2, \dots, a_m) = [a_1^\top, a_2^\top, \dots, a_m^\top]^\top$ . Given matrices of the same column size  $A_1, A_2, \dots, A_m$ , we denote  $\text{col}(A_1, A_2, \dots, A_m) = [A_1^\top, A_2^\top, \dots, A_m^\top]^\top$ . Denote  $\text{diag}(x_1, \dots, x_m)$  as a diagonal matrix with  $x_1, \dots, x_m$  on its diagonal entries and  $\text{diag}(D_1, \dots, D_m)$  as a block-diagonal matrix with matrices  $D_1, \dots, D_m$  on its diagonal blocks. We use  $e_n^i$  to denote an  $n \times 1$  unit vector, with the  $i$ th entry being one and the others being zeros. Finally,  $A \otimes B$  represents the Kronecker product between matrices  $A$  and  $B$ .

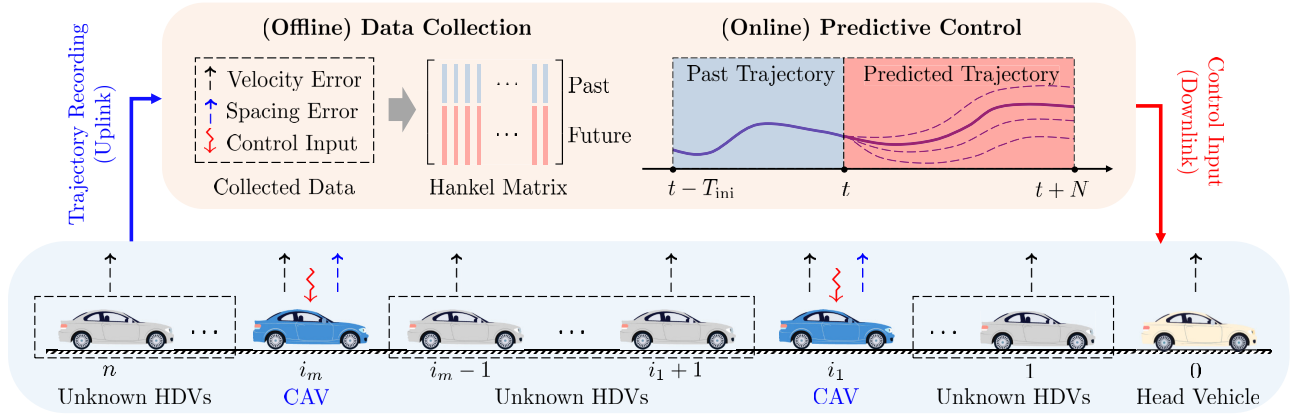


Fig. 1. Schematic of DeeP-LCC for CAVs in mixed traffic. The head vehicle is located at the beginning, indexed as 0, behind which there exist  $n$  vehicles indexed from 1 to  $n$ . The  $n$  vehicles consist of  $n - m$  HDVs, whose car-following dynamics are unknown, and  $m$  CAVs, indexed from  $i_1$  to  $i_m$ . In (offline) data collection, DeeP-LCC records measurable data of the mixed traffic system, including velocity errors of each vehicle (represented by the black dashed arrow) and spacing errors of the CAVs (represented by the blue dashed arrow). Then, DeeP-LCC utilizes these data to construct Hankel matrices for future trajectory predictions. In (online) predictive control, DeeP-LCC employs the collected data to design the optimal future trajectory and sends the control signal to the CAVs (represented by the red squiggle arrow). Details on DeeP-LCC are presented in Section V.

## II. THEORETICAL MODELING FRAMEWORK

In this section, we first introduce the nonlinear modeling of HDVs' car-following behavior and then present the linearized dynamics of a general mixed traffic system under the LCC framework [11].

As shown in Fig. 1, we consider a general mixed traffic system with  $n + 1$  individual vehicles, among which there exist one head vehicle, indexed as 0, and  $m$  CAVs and  $n - m$  HDVs in the following  $n$  vehicles, indexed from 1 to  $n$ . Note that essentially, any HDV ahead of the first CAV can be designated as the head vehicle. Define  $\Omega = \{1, 2, \dots, n\}$  as the index set of all the following vehicles, ordered from front to end, and  $S = \{i_1, i_2, \dots, i_m\} \subseteq \Omega$  as the set of the CAV indices, where  $i_1 < i_2 < \dots < i_m$  also represent the spatial locations of the CAVs in the mixed traffic. The position, velocity, and acceleration of the  $i$ th vehicle at time  $t$  are denoted as  $p_i(t)$ ,  $v_i(t)$ , and  $a_i(t)$ , respectively.

### A. Nonlinear Car-Following Dynamics of HDVs

There are many well-established models to describe car-following dynamics of HDVs, such as the optimal velocity model (OVM) [36], and the intelligent driver model (IDM) [37]. These models can capture various human driving behaviors and reproduce typical traffic phenomena, e.g., stop-and-go traffic waves [38].

In these models, the acceleration of an HDV depends on its car-following spacing  $s_i(t) = p_{i-1}(t) - p_i(t)$ , i.e., the bumper-to-bumper distance between vehicle  $i$  and its preceding vehicle  $i - 1$ , its relative velocity  $\dot{s}_i(t) = v_{i-1}(t) - v_i(t)$ , and its own velocity  $v_i(t)$ . A typical form is [39]

$$\dot{v}_i(t) = F(s_i(t), \dot{s}_i(t), v_i(t)), \quad i \in \Omega \setminus S \quad (1)$$

where  $F(\cdot)$  is a nonlinear function. Both OVM and IDM can be written in this general form. Here, we use the OVM model to exemplify the HDVs' car-following behavior in (1), which has been widely considered in [13], [16], [22], and [35]. In

OVM, the dynamics (1) are

$$\dot{v}_i(t) = \alpha(v_{\text{des}}(s_i(t)) - v_i(t)) + \beta \dot{s}_i(t), \quad i \in \Omega \setminus S \quad (2)$$

where  $\alpha, \beta > 0$  denote the driver's sensitivity coefficients, and  $v_{\text{des}}(s)$  represents the spacing-dependent desired velocity of the human driver, given by a continuous piecewise function

$$v_{\text{des}}(s) = \begin{cases} 0, & s \leq s_{\text{st}} \\ f_v(s), & s_{\text{st}} < s < s_{\text{go}} \\ v_{\text{max}}, & s \geq s_{\text{go}}. \end{cases} \quad (3)$$

In (3), the desired velocity  $v_{\text{des}}(s)$  becomes zero for a small spacing  $s_{\text{st}}$  and reaches a maximum value  $v_{\text{max}}$  for a large spacing  $s_{\text{go}}$ . When  $s_{\text{st}} < s < s_{\text{go}}$ , the desired velocity is given by a monotonically increasing function  $f_v(s)$ , one typical choice of which is

$$f_v(s) = \frac{v_{\text{max}}}{2} \left( 1 - \cos \left( \pi \frac{s - s_{\text{st}}}{s_{\text{go}} - s_{\text{st}}} \right) \right). \quad (4)$$

In the following, we proceed to use the general form (1) of the car-following model to present the parametric system modeling and controllability/observability analysis.

### B. Input-Output of Mixed Traffic System

We now present the state, output, and input vectors of the mixed traffic system shown in Fig. 1.

1) *Equilibrium Traffic State*: In an equilibrium traffic state, each vehicle moves with the same velocity  $v^*$  and the corresponding spacing  $s^*$ . When each vehicle follows its predecessor, as shown in Fig. 1, the equilibrium velocity of the traffic system is determined by the steady-state velocity of the head vehicle, indexed as 0. If the head vehicle maintains a constant velocity  $v_0$ , we have  $v^* = v_0$  for all other vehicles in Fig. 1.

On the other hand, the equilibrium spacing for each vehicle might be heterogeneous<sup>1</sup> and can be nontrivial to obtain.

<sup>1</sup>We keep  $s^*$  instead of a heterogeneous symbol  $s_i^*$ ,  $i \in \{1, 2, \dots, n\}$  for notational simplicity. Our methodology and results are directly applicable in the heterogeneous case.

If the HDVs' car-following dynamics (1) are explicitly known, we can obtain the equilibrium spacing via solving

$$F(s^*, 0, v^*) = 0 \quad (5)$$

which provides equilibrium points  $(s^*, v^*)$ . However,  $s^*$  becomes unknown if (1) is not known accurately. The equilibrium spacing for each CAV is a predesigned variable [6].

2) *System State*: Assuming that the mixed traffic flow is moving around an equilibrium state  $(s^*, v^*)$ , we define the error state between the actual and the equilibrium point as  $(i \in \Omega)$

$$\tilde{s}_i(t) = s_i(t) - s^*, \quad \tilde{v}_i(t) = v_i(t) - v^* \quad (6)$$

where  $\tilde{s}_i(t)$  and  $\tilde{v}_i(t)$  represent the spacing error and velocity error of vehicle  $i$  at time  $t$ , respectively. The error states of all the vehicles are then lumped as the mixed traffic system state  $x(t) \in \mathbb{R}^{2n}$  that is given by

$$x(t) = [\tilde{s}_1(t), \tilde{v}_1(t), \tilde{s}_2(t), \tilde{v}_2(t), \dots, \tilde{s}_n(t), \tilde{v}_n(t)]^\top. \quad (7)$$

3) *System Output*: Not all the variables in mixed traffic state  $x(t)$  can be measured. As discussed above, the equilibrium spacing  $s^*$  for the HDVs is nontrivial to get accurately due to unknown car-following dynamics (1). It is thus impractical to observe the spacing errors of the HDVs, i.e.,  $\tilde{s}_i(t)$  ( $i \notin S$ ). For the CAVs, their equilibrium spacing can be designed [6], and thus, their spacing error signal can be measured.

We thus introduce the following output signal:

$$y(t) = [\tilde{v}_1(t), \tilde{v}_2(t), \dots, \tilde{v}_n(t), \tilde{s}_{i_1}(t), \tilde{s}_{i_2}(t), \dots, \tilde{s}_{i_m}(t)]^\top \quad (8)$$

where  $y(t) \in \mathbb{R}^{n+m}$  consists of all measurable data, including the velocity errors of both the HDVs and the CAVs, i.e.,  $\tilde{v}_i(t)$  ( $i \in \Omega$ ), and the spacing errors of all the CAVs, i.e.,  $\tilde{s}_i(t)$  ( $i \in S$ ). The measurable output data are also marked in Fig. 1, with velocity errors and spacing errors represented by black dashed arrows and blue dashed arrows, respectively.

4) *System Input*: In mixed traffic flow, the HDVs are controlled by human drivers, while the CAVs' behavior can be designed. As used in [6], [13], [16], [22], and [35], the acceleration of each CAV is assumed to be directly controlled

$$\dot{v}_i(t) = u_i(t), \quad i \in S \quad (9)$$

where  $u_i(t)$  is the control input of the CAV indexed as  $i$ . The acceleration signals of all the CAVs are lumped as the aggregate control input  $u(t) \in \mathbb{R}^m$  that is given by

$$u(t) = [u_{i_1}(t), u_{i_2}(t), \dots, u_{i_m}(t)]^\top. \quad (10)$$

In addition to the control input, we introduce an external input signal  $\epsilon(t) \in \mathbb{R}$  of the mixed traffic system, which is defined as the velocity error of the head vehicle, which is given by

$$\epsilon(t) = \tilde{v}_0(t) = v_0(t) - v^*. \quad (11)$$

This external input signal plays a critical role in our subsequent system analysis and Deep-LCC design. Since the head vehicle

is also under human control, this input cannot be designed directly, but its past value can be measured and future value can be estimated.

### C. Linearized State-Space Model of Mixed Traffic System

After specifying the system state, input, and output, we now present a linearized mixed traffic model. Using (5) and applying the first-order Taylor expansion to (1), we obtain the following linearized model for each HDV

$$\begin{cases} \dot{\tilde{s}}_i(t) = \tilde{v}_{i-1}(t) - \tilde{v}_i(t), \\ \dot{\tilde{v}}_i(t) = \alpha_1 \tilde{s}_i(t) - \alpha_2 \tilde{v}_i(t) + \alpha_3 \tilde{v}_{i-1}(t), \end{cases} \quad i \in \Omega \setminus S \quad (12)$$

where  $\alpha_1 = (\partial F / \partial s)$ ,  $\alpha_2 = (\partial F / \partial \dot{s}) - (\partial F / \partial v)$ , and  $\alpha_3 = (\partial F / \partial \dot{s})$  with the partial derivatives evaluated at the equilibrium state  $(s^*, v^*)$ . To reflect asymptotically stable driving behaviors of human drivers, we have  $\alpha_1 > 0$  and  $\alpha_2 > \alpha_3 > 0$  [16]. Taking the OVM model (2) for example, the equilibrium equation (5) is given by

$$v_{\text{des}}(s^*) = v^* \quad (13)$$

and the coefficients in the linearized dynamics (12) become

$$\alpha_1 = \alpha \dot{v}_{\text{des}}(s^*), \quad \alpha_2 = \alpha + \beta, \quad \alpha_3 = \beta$$

where  $\dot{v}_{\text{des}}(s^*)$  denotes the derivative of  $v_{\text{des}}(s)$  at the equilibrium spacing  $s^*$ .

For the CAV, we consider a second-order model

$$\begin{cases} \dot{\tilde{s}}_i(t) = \tilde{v}_{i-1}(t) - \tilde{v}_i(t) \\ \dot{\tilde{v}}_i(t) = u_i(t), \end{cases} \quad i \in S. \quad (14)$$

Based on the state, output, and input vectors in (6)–(11), the linearized HDVs' car-following model (12), and the CAV's dynamics (14), we derive a linearized state-space model of the mixed traffic in Fig. 1 as

$$\begin{cases} \dot{x}(t) = Ax(t) + Bu(t) + H\epsilon(t) \\ y(t) = Cx(t). \end{cases} \quad (15)$$

In (15), the matrices  $A \in \mathbb{R}^{2n \times 2n}$ ,  $B \in \mathbb{R}^{2n \times m}$ ,  $H \in \mathbb{R}^{2n \times 1}$ , and  $C \in \mathbb{R}^{(n+m) \times 2n}$  are given by

$$A = \begin{bmatrix} A_{1,1} & & & & \\ A_{2,2} & A_{2,1} & & & \\ & \ddots & \ddots & & \\ & & A_{n-1,2} & A_{n-1,1} & \\ & & & A_{n,2} & A_{n,1} \end{bmatrix}$$

$$B = [\mathbf{e}_{2n}^{2i_1}, \mathbf{e}_{2n}^{2i_2}, \dots, \mathbf{e}_{2n}^{2i_m}], \quad H = [h_1^\top, h_2^\top, \dots, h_n^\top]^\top$$

$$C = [\mathbf{e}_{2n}^{2i_1}, \mathbf{e}_{2n}^{4i_1}, \dots, \mathbf{e}_{2n}^{2i_1-1}, \mathbf{e}_{2n}^{2i_2-1}, \dots, \mathbf{e}_{2n}^{2i_m-1}]^\top$$

where<sup>2</sup>

$$A_{i,1} = \begin{cases} P_1, & i \notin S \\ S_1, & i \in S \end{cases} \quad A_{i,2} = \begin{cases} P_2, & i \notin S \\ S_2, & i \in S \end{cases}$$

$$h_1 = \begin{bmatrix} 1 \\ \alpha_3 \end{bmatrix}, \quad h_j = \begin{bmatrix} 0 \\ 0 \end{bmatrix}, \quad j \in \{2, 3, \dots, n\}$$

with

$$P_1 = \begin{bmatrix} 0 & -1 \\ \alpha_1 & -\alpha_2 \end{bmatrix}, \quad P_2 = \begin{bmatrix} 0 & 1 \\ 0 & \alpha_3 \end{bmatrix}, \quad S_1 = \begin{bmatrix} 0 & -1 \\ 0 & 0 \end{bmatrix}, \quad S_2 = \begin{bmatrix} 0 & 1 \\ 0 & 0 \end{bmatrix}.$$

<sup>2</sup>The system matrices  $A$ ,  $B$ , and  $C$  are indeed set functions with respect to the value of  $S$  [7]. For simplicity, the symbol  $S$  is neglected.



*Remark 1 (State Feedback Versus Output Feedback):* Most existing work on CAV control relies on state feedback, which assumes a known equilibrium spacing  $s^*$  and requires the system state  $x(t)$  in (7) (see, e.g., the model-based strategies [6], [16], [35] and the data-driven strategies [21], [22], [24]). The output-feedback case has been less investigated (two notable exceptions are [13] and [40]). In practice, the equilibrium spacing  $s^*$  is unknown and might be time-varying. Hence, we introduce a measurable output in (8) that does not use the HDVs' spacing errors. Also, the CAVs' spacing errors play a critical role in car-following safety, and they should be constrained for collision-free guarantees. The output-feedback and constraint requirements motivate us to use an MPC framework later.  $\square$

*Remark 2 (Unknown Car-Following Behavior):* One challenge for mixed traffic control lies in the unknown car-following behavior (1). After linearization, the state-space model (15) of the mixed traffic system remains unknown. We focus on a data-driven predictive control method that directly relies on the driving data of HDVs. Before presenting the methodology, we need to investigate two fundamental control-theoretic properties of the mixed traffic system, controllability and observability, which are essential to establish data-driven predictive control [26]. Our previous work on LCC has investigated the special case with only one CAV [11]. In Section III, we generalize these results to the case with possibly multiple CAVs and HDVs coexisting (see Fig. 1).  $\square$

### III. CONTROLLABILITY AND OBSERVABILITY OF MIXED TRAFFIC SYSTEMS

Controllability and observability are two fundamental properties in dynamical systems [41]. For mixed traffic systems, existing research [11], [16] has revealed the controllability for the scenario of one single CAV and multiple HDVs, i.e.,  $|S| = 1$ . These results have been unified in the recent LCC framework with one single CAV [11].

*Lemma 1 [11, Corollary 1]:* When  $S = \{1\}$ , the linearized mixed traffic system (15) is controllable if we have

$$\alpha_1 - \alpha_2\alpha_3 + \alpha_3^2 \neq 0. \quad (16)$$

*Lemma 2 [11, Th. 2]:* When  $S = \{i_1\}$  with  $1 < i_1 \leq n$ , the linearized mixed traffic system (15) is not controllable but is stabilizable, if (16) holds. Moreover, if (16) holds the subsystem consisting of the states  $\tilde{s}_1, \tilde{v}_1, \dots, \tilde{s}_{i_1-1}, \tilde{v}_{i_1-1}$  is not controllable but is stable, while the subsystem consisting of the states  $\tilde{s}_{i_1}, \tilde{v}_{i_1}, \dots, \tilde{s}_n, \tilde{v}_n$  is controllable.

One physical interpretation of Lemmas 1 and 2 is that the control input of the single CAV has no influence on the state of its preceding HDVs but has full control of the motion of its following HDVs when (16) holds.

We now present the controllability properties of the general mixed traffic system with multiple CAVs and HDVs in Fig. 1.

*Theorem 1 (Controllability):* Consider the mixed traffic system (15), where there exist  $m$  ( $m \geq 1$ ) CAVs with indices  $S = \{i_1, i_2, \dots, i_m\}$ ,  $i_1 < i_2 < \dots < i_m$ . We have the following.

- 1) When  $1 \in S$ , i.e.,  $i_1 = 1$ , the mixed traffic system is controllable if (16) holds.

- 2) When  $1 \notin S$ , i.e.,  $i_1 > 1$ , the mixed traffic system is not controllable but is stabilizable, if (16) holds. In particular, when (16) holds, the subsystem consisting of the states  $\tilde{s}_1, \tilde{v}_1, \dots, \tilde{s}_{i_1-1}, \tilde{v}_{i_1-1}$  is not controllable but is stable, while the subsystem consisting of the states  $\tilde{s}_{i_1}, \tilde{v}_{i_1}, \dots, \tilde{s}_n, \tilde{v}_n$  is controllable.

*Proof:* The proof combines the controllability invariance after state feedback with Lemmas 1 and 2. The details are not mathematically involved, and we provide them in Appendix A for completeness.  $\blacksquare$

This result indicates that the general mixed traffic system consisting of multiple CAVs and HDVs is not controllable (but stabilizable) unless the vehicle immediately behind the head vehicle is a CAV. This is expected since the motion of the HDVs between the head vehicle and the first CAV (i.e., vehicles indexed from 1 to  $i_1 - 1$ ) cannot be influenced by the CAVs' control inputs.

We consider an output-feedback controller design. It is essential to evaluate the observability of the mixed traffic system (15). The notion of observability quantifies the ability of reconstructing the system state from its output measurements. By adapting [11, Th. 4], we have the following result.

*Theorem 2 (Observability):* The general mixed traffic system given by (15), where there exist  $m$  ( $m \geq 1$ ) CAVs, is observable when (16) holds.

The slight asymmetry between Theorems 1 and 2 is due to the fact that the control input (10) only includes the CAVs' acceleration, while the system output (8) consists of the velocity error of all the vehicles and the spacing error of the CAVs. Theorem 2 reveals the observability of the full state  $x(t)$  in mixed traffic under a mild condition. This observability result facilitates the design of our DeeP-LCC strategy, which will be detailed in Sections IV and V.

### IV. DATA-ENABLED PREDICTIVE CONTROL

In this section, we give an overview of the data-driven methodology on nonparametric representation of system behavior and data-enabled predicted control; more details can be referred to [26] and [30].

#### A. Nonparametric Representation of System Behavior

DeePC works on discrete-time systems [26]. Let us consider a discrete-time LTI system

$$\begin{cases} x(k+1) = A_d x(k) + B_d u(k) \\ y(k) = C_d x(k) + D_d u(k) \end{cases} \quad (17)$$

where  $A_d \in \mathbb{R}^{n \times n}$ ,  $B_d \in \mathbb{R}^{n \times m}$ ,  $C_d \in \mathbb{R}^{p \times n}$ ,  $D_d \in \mathbb{R}^{p \times m}$ , and  $x(k) \in \mathbb{R}^n$ ,  $u(k) \in \mathbb{R}^m$ , and  $y(k) \in \mathbb{R}^p$  denote the internal state, control input, and output at time  $k$  ( $k \in \mathbb{N}$ ), respectively. By slight abuse of notation, we use the symbols  $n, m$ , and  $p$  to denote system dimensions only in this section.

Classical control strategies typically follow the sequential system identification and model-based controller design. They rely on the explicit system model  $A_d, B_d, C_d$ , and  $D_d$  in (17). One typical strategy is the celebrated MPC framework [23]. The performance of MPC is closely related to the accuracy

of the system model. Although many system identification methods are available [42], it is still nontrivial to obtain an accurate model for complex systems, e.g., the mixed traffic system with complex nonlinear human driving behavior. The recent DeePC [26] is a nonparametric method that bypasses system identification and directly designs the control input compatible with historical data. In particular, DeePC directly uses historical data to predict the system behavior based on Willems' fundamental lemma [27].

**Definition 1:** The signal  $\omega = \text{col}(\omega(1), \omega(2), \dots, \omega(T))$  of length  $T$  ( $T \in \mathbb{N}$ ) is persistently exciting of order  $l$  ( $l \leq T$ ,  $l \in \mathbb{N}$ ) if the following Hankel matrix:

$$\mathcal{H}_l(\omega) := \begin{bmatrix} \omega(1) & \omega(2) & \cdots & \omega(T-l+1) \\ \omega(2) & \omega(3) & \cdots & \omega(T-l+2) \\ \vdots & \vdots & \ddots & \vdots \\ \omega(l) & \omega(l+1) & \cdots & \omega(T) \end{bmatrix} \quad (18)$$

is of full row rank.

William's fundamental lemma begins by collecting a length- $T$  ( $T \in \mathbb{N}$ ) sequence of trajectory data from system (17), consisting of the input sequence  $u^d = \text{col}(u^d(1), \dots, u^d(T)) \in \mathbb{R}^{mT}$  and the corresponding output sequence  $y^d = \text{col}(y^d(1), \dots, y^d(T)) \in \mathbb{R}^{pT}$ . Then, it aims to utilize this precollected length- $T$  trajectory to directly construct valid length- $L$  ( $L \in \mathbb{N}$ ) trajectories of the system, consisting of input sequence  $u^s \in \mathbb{R}^{mL}$  and output sequence  $y^s \in \mathbb{R}^{pL}$ .

**Lemma 3 (Fundamental Lemma [27]):** Consider a controllable LTI system (17) and assume the input sequence  $u^d$  to be persistently exciting of order  $L + n$ . Then,  $(u^s, y^s)$  is a length- $L$  input-output trajectory of system (17) if and only if there exists  $g \in \mathbb{R}^{T-L+1}$  such that

$$\begin{bmatrix} \mathcal{H}_L(u^d) \\ \mathcal{H}_L(y^d) \end{bmatrix} g = \begin{bmatrix} u^s \\ y^s \end{bmatrix}. \quad (19)$$

This fundamental lemma reveals that given a controllable LTI system, the subspace consisting of all valid length- $L$  trajectories is identical to the range space of the Hankel matrix of depth  $L$  generated by a sufficiently rich input signal. Rather than identifying a parametric model, this lemma allows for nonparametric representation of system behaviors.

### B. Data-Enabled Predictive Control

Define  $T_{\text{ini}} \in \mathbb{N}$  and  $N \in \mathbb{N}$  as the time length of "past data" and "future data", respectively. The data Hankel matrices constructed from the precollected data  $(u^d, y^d)$  are partitioned into the two parts (corresponding to past data and future data)

$$\begin{bmatrix} U_p \\ U_f \end{bmatrix} := \mathcal{H}_{T_{\text{ini}}+N}(u^d), \quad \begin{bmatrix} Y_p \\ Y_f \end{bmatrix} := \mathcal{H}_{T_{\text{ini}}+N}(y^d) \quad (20)$$

where  $U_p$  and  $U_f$  consist of the first  $T_{\text{ini}}$  block rows and the last  $N$  block rows of  $\mathcal{H}_{T_{\text{ini}}+N}(u^d)$ , respectively (similar to  $Y_p$  and  $Y_f$ ). The same column in  $\text{col}(U_p, U_f)$  and  $\text{col}(Y_p, Y_f)$  represents the "past" input-output signal of length  $T_{\text{ini}}$  and the "future" input-output signal of length  $N$  within a length- $(T_{\text{ini}} + N)$  trajectory of (17).

At time step  $t$ , we define  $u_{\text{ini}} = \text{col}(u(t - T_{\text{ini}}), u(t - T_{\text{ini}} + 1), \dots, u(t - 1))$ ,  $u = \text{col}(u(t), u(t + 1), \dots,$

### Algorithm 1 DeePC [26]

---

**Input:** Offline data  $(u^d, y^d)$ , initial time  $t_0$ , final time  $t_f$ ;  
1: Construct data Hankel matrices  $U_p, U_f, Y_p, Y_f$ ;  
2: Initialize past data  $(u_{\text{ini}}, y_{\text{ini}})$  before time  $t_0$ ;  
3: **while**  $t_0 \leq t \leq t_f$  **do**  
4:   Solve (22) to get an optimal input sequence  $u^* = \text{col}(u^*(t), u^*(t+1), \dots, u^*(t+N-1))$ ;  
5:   Apply the input  $u(t) \leftarrow u^*(t)$ ;  
6:    $t \leftarrow t+1$  and update past input/output data  $(u_{\text{ini}}, y_{\text{ini}})$ ;  
7: **end while**

---

$u(t+N-1))$  as the past control input sequence with time length  $T_{\text{ini}}$  and the future control input sequence with time horizon  $N$ , respectively (similar to  $y_{\text{ini}}, y$ ). Then, we have the following proposition, which is a reformulation of Lemma 3.

**Proposition 1 [43]:** Consider a controllable LTI system (17) and assume the input sequence  $u^d$  to be persistently exciting of order  $T_{\text{ini}} + N + n$ . Then,  $\text{col}(u_{\text{ini}}, u, y_{\text{ini}}, y)$  is a length- $(T_{\text{ini}} + N)$  input-output trajectory of system (17) if and only if there exists  $g \in \mathbb{R}^{T-T_{\text{ini}}-N+1}$  such that

$$\begin{bmatrix} U_p \\ Y_p \\ U_f \\ Y_f \end{bmatrix} g = \begin{bmatrix} u_{\text{ini}} \\ y_{\text{ini}} \\ u \\ y \end{bmatrix}. \quad (21)$$

In particular, if  $T_{\text{ini}} \geq \nu$ , where  $\nu$  denotes the lag<sup>3</sup> of system (17),  $y$  is unique from (21),  $\forall u_{\text{ini}}, y_{\text{ini}}, u$ .

A schematic of Proposition 1 is shown in Fig. 2. The formulation (21) indicates that given a past input-output trajectory  $(u_{\text{ini}}, y_{\text{ini}})$ , one can predict the future output sequence  $y$  under a future input sequence  $u$  directly from precollected data  $(u^d, y^d)$ . It is known that when  $T_{\text{ini}} \geq \nu$ , one can estimate the initial state based on model (17) and the past input-output trajectory  $(u_{\text{ini}}, y_{\text{ini}})$ . Thus, (21) implicitly estimates the initial state to predict the future trajectory  $\text{col}(u, y)$  without an explicit parametric model [26].

At each time step  $t$ , DeePC relies on the data-centric representation (21) to predict future system behavior and solves the following optimization problem [26]:

$$\begin{aligned} \min_{g, u, y} \quad & J(y, u) \\ \text{s.t.} \quad & (21), u \in \mathcal{U}, y \in \mathcal{Y} \end{aligned} \quad (22)$$

where  $J(y, u)$  denotes the control objective function, and  $u \in \mathcal{U}$  and  $y \in \mathcal{Y}$  represent the input-output constraints, e.g., safety guarantees and control saturation. Problem (22) is solved in a receding horizon manner (see Algorithm 1). For comparison, we also present a standard output-feedback MPC

$$\begin{aligned} \min_u \quad & J(y, u) \\ \text{s.t.} \quad & x(t) = \hat{x}(t) \\ & (17) \quad \forall k \in \{t, t+1, \dots, t+N-1\} \\ & u \in \mathcal{U}, y \in \mathcal{Y} \end{aligned} \quad (23)$$

where  $\hat{x}(t)$  denotes the estimated initial state at time  $t$ .

<sup>3</sup>The lag  $\nu$  of a system  $(A, B, C, D)$  is the smallest integer such that the observability matrix  $\text{col}(C, CA, \dots, CA^{\nu-1})$  has full column rank.

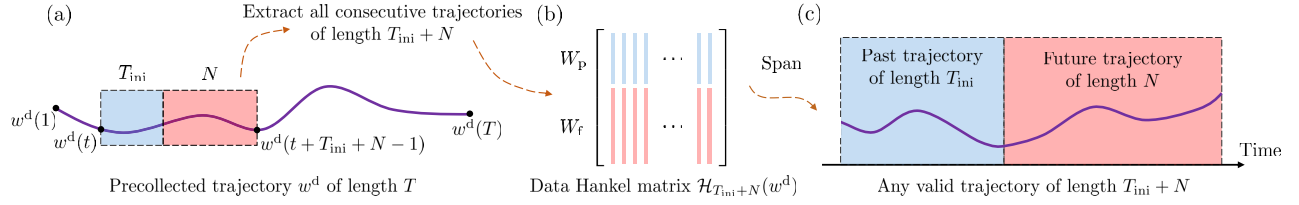


Fig. 2. Interpretation of the fundamental lemma in (21). Here, we use  $w$  to denote input–output trajectory pair  $(u, y)$ . (a) Consecutive length- $T$  trajectory is collected  $w^d = \text{col}(w^d(1), \dots, w^d(T))$ . (b) All consecutive length- $(T_{ini} + N)$  trajectories are extracted to construct the data Hankel matrix  $\mathcal{H}_{T_{ini}+N}(w^d)$ . In particular, each trajectory is partitioned into two parts, past data of length  $T_{ini}$  colored in blue and future data of length  $T$  colored in red. (c) Range space of this data Hankel matrix contains all valid length- $(T_{ini} + N)$  trajectories of the underlying system.

Despite its well-recognized effectiveness, one crucial challenge for the standard MPC (23) is the requirement of an explicit parametric model (17), which is necessary in estimating the initial state  $\hat{x}(t)$  and predicting future system behaviors. In contrast, DeePC (22) focuses on the data-centric nonparametric representation and bypasses the state estimation procedure [26]. Recent work has revealed the equivalence between DeePC and sequential system identification and MPC for discrete-time LTI systems under mild conditions and comparable performance of DeePC with respect to MPC based on accurate model knowledge in applications to nonlinear and nondeterministic systems [30].

#### V. DEEP-LCC FOR MIXED TRAFFIC FLOW

Willems' fundamental lemma requires the controllability of the discrete-time LTI system (17) and the persistent excitation of precollected input data  $u^d$  [27]. As shown in Theorem 1, the mixed traffic system is not always controllable, and thus, the original DeePC cannot be directly applied for mixed traffic control.

In this section, we introduce an external input signal for mixed traffic. Together with original control input, this leads to controllability. We first reformulate mixed traffic model (15) and then present DeeP-LCC for mixed traffic control.

##### A. Model Reformulation With External Input

Theorem 1 has revealed that the mixed traffic system (15) is not controllable when  $1 \notin S$ , i.e., the first vehicle behind the head vehicle is not a CAV. Still, controllability is a desired property, which is required in Willems' fundamental lemma (Lemma 3) to guarantee the data-centric behavior representation. To resolve this, we introduce a variant of the original system (15) that is fully controllable.

The velocity error of the head vehicle  $\epsilon(t) = v_0(t) - v^*$  is an external input in (15). This signal is not directly controlled but can be measured in practice. Define  $\hat{u}(t) = \text{col}(\epsilon(t), u(t))$  as a combined input signal and  $\hat{B} = [H, B]$  as the corresponding input matrix. The model for the mixed traffic system becomes

$$\begin{cases} \dot{x}(t) = Ax(t) + \hat{B}\hat{u}(t) \\ y(t) = Cx(t) \end{cases} \quad (24)$$

for which we have the following result.

**Corollary 1 (Controllability and Observability of the Reformulated Traffic Model):** Suppose that there exist  $m$  ( $m \geq 1$ )

CAVs. Then, system (24) is controllable and observable if (16) holds.

The proof is similar to that of the system when the first vehicle behind the head vehicle is a CAV [11], i.e.,  $1 \in S$ ; we refer the interested reader to [11, Corollary 1]. For observability, it is immediate to see that system (24) shares the same output dynamics as system (15), whose observability result has been proved in Theorem 2.

By Corollary 1, we can apply the fundamental lemma using a combined input  $\hat{u}(t)$  consisting of the internal control input (i.e., the acceleration signals  $u(t)$  of the CAVs) and the external input (i.e., the velocity error  $\epsilon(t)$  of the head vehicle). For simplicity, we use the original system model (15) where the two input signals  $u(t)$  and  $\epsilon(t)$  are still separated. Finally, the system model (15) is in the continuous-time domain. We transform it to the discrete-time domain

$$\begin{cases} x(k+1) = A_d x(k) + B_d u(k) + H_d \epsilon(k) \\ y(k) = C_d x(k) \end{cases} \quad (25)$$

where  $A_d = e^{A\Delta t} \in \mathbb{R}^{2n \times 2n}$ ,  $B_d = \int_0^{\Delta t} e^{A\tau} B d\tau \in \mathbb{R}^{2n \times m}$ ,  $H_d = \int_0^{\Delta t} e^{A\tau} H d\tau \in \mathbb{R}^{2n \times 1}$ ,  $C_d = C \in \mathbb{R}^{(n+m) \times 2n}$ , and  $\Delta t > 0$  is the sampling time interval.

**Assumption 1:** Denote  $\lambda_i$ ,  $i = 1, \dots, 2n$ , as the eigenvalues of  $A$  in the continuous-time mixed traffic system model (15). We have  $|\text{Im}[\lambda_i - \lambda_j]| \neq 2\pi k/\Delta t$ ,  $k = 1, 2, \dots$ , whenever  $\text{Re}[\lambda_i - \lambda_j] = 0$ ,  $i, j = 1, \dots, 2n$ .

As revealed in [44, Th. 6.9], Assumption 1 is a sufficient condition to preserve controllability and observability after discretization from (15) to the discrete-time system model (25).

##### B. Nonparametric Representation of Mixed Traffic Behavior

**1) Data Collection:** We begin by collecting the length- $T$  trajectory data from the mixed traffic system shown in Fig. 1. Precisely, the collected data include the following.

- 1) The combined input sequence  $\hat{u}^d = \text{col}(\hat{u}^d(1), \dots, \hat{u}^d(T)) \in \mathbb{R}^{(m+1)T}$ , consisting of CAVs' acceleration sequence  $u^d = \text{col}(u^d(1), \dots, u^d(T)) \in \mathbb{R}^{mT}$  and the velocity error sequence of the head vehicle  $\epsilon^d = \text{col}(\epsilon^d(1), \dots, \epsilon^d(T)) \in \mathbb{R}^T$ ;
- 2) The corresponding output sequence of the mixed traffic system  $y^d = \text{col}(y^d(1), \dots, y^d(T)) \in \mathbb{R}^{(n+m)T}$ .

The precollected data are then partitioned into two parts, corresponding to "past data" of length  $T_{ini}$  and "future data"

of length  $N$ . Precisely, define

$$\begin{bmatrix} U_p \\ U_f \end{bmatrix} := \mathcal{H}_{T_{\text{ini}}+N}(u^d), \quad \begin{bmatrix} E_p \\ E_f \end{bmatrix} := \mathcal{H}_{T_{\text{ini}}+N}(\epsilon^d) \\ \begin{bmatrix} Y_p \\ Y_f \end{bmatrix} := \mathcal{H}_{T_{\text{ini}}+N}(y^d) \quad (26)$$

where  $U_p$  and  $U_f$  consist of the first  $T_{\text{ini}}$  block rows and the last  $N$  block rows of  $\mathcal{H}_{T_{\text{ini}}+N}(u^d)$ , respectively (similar to  $E_p$  and  $E_f$  and  $Y_p$  and  $Y_f$ ).

These precollected data samples could be generated offline or collected from the historical trajectories of those involved vehicles. According to Lemma 3, the following assumption is needed for the precollected data (recall that the order of the mixed traffic system is  $2n$ ).

**Assumption 2:** The combined input sequence  $\hat{u}^d$  is persistently exciting of order  $T_{\text{ini}} + N + 2n$ .  $\square$

Note that the external input, i.e., the velocity error of the head vehicle  $\epsilon(t)$ , is controlled by a human driver. Although it cannot be arbitrarily designed, it is always oscillating around zero since the driver always attempts to maintain the equilibrium velocity while suffering from small perturbations. Thus, given a trajectory with length

$$T \geq (m+1)(T_{\text{ini}} + N + 2n) - 1 \quad (27)$$

which allows for a  $\hat{u}^d$  Hankel matrix of order  $T_{\text{ini}} + N + 2n$  to have a larger column number than the row number and persistently exciting acceleration input  $u(t)$  of the CAVs (e.g., independent and identically distributed (i.i.d.) noise with zero mean), the persistent excitation in Assumption 2 is naturally satisfied.

**2) Behavior Representation:** Similar to Proposition 1, we have the following result. At time step  $t$ , define

$$u_{\text{ini}} = \text{col}(u(t - T_{\text{ini}}), u(t - T_{\text{ini}} + 1), \dots, u(t - 1)) \\ u = \text{col}(u(t), u(t + 1), \dots, u(t + N - 1)) \quad (28)$$

as the control sequence within a past time length  $T_{\text{ini}}$  and the control sequence within a predictive time length  $N$ , respectively (similar to  $\epsilon_{\text{ini}}$  and  $\epsilon$  and  $y_{\text{ini}}$  and  $y$ ).

**Proposition 2:** Suppose that (16) and Assumptions 1 and 2 hold. Any length- $(T_{\text{ini}} + N)$  trajectory of the mixed traffic system (25), denoted as  $\text{col}(u_{\text{ini}}, \epsilon_{\text{ini}}, y_{\text{ini}}, u, \epsilon, y)$ , can be constructed via

$$\begin{bmatrix} U_p \\ E_p \\ Y_p \\ U_f \\ E_f \\ Y_f \end{bmatrix} g = \begin{bmatrix} u_{\text{ini}} \\ \epsilon_{\text{ini}} \\ y_{\text{ini}} \\ u \\ \epsilon \\ y \end{bmatrix} \quad (29)$$

where  $g \in \mathbb{R}^{T-T_{\text{ini}}-N+1}$ . If  $T_{\text{ini}} \geq 2n$ ,  $y$  is unique from (29),  $\forall u_{\text{ini}}, \epsilon_{\text{ini}}, y_{\text{ini}}, u, \epsilon$ .

**Proof:** Condition (16) and Assumption 1 guarantee the controllability and observability of the mixed traffic system (25), and Assumption 2 offers the persistent excitation property of precollected data. Then, this result can be derived from Proposition 1. Since the mixed traffic system is observable under condition (16), its lag is not larger than its state

dimension  $2n$ , and thus, we have the uniqueness of  $y$  by Proposition 1.  $\blacksquare$

Proposition 2 reveals that by collecting traffic data, one can directly predict the future trajectory of the mixed traffic system. We thus require no explicit model of HDVs' car-following behavior. Note that HDVs are controlled by human drivers and have complex and uncertain dynamics. This result allows us to bypass a parametric system model and directly use nonparametric data-centric representation for the behavior of the mixed traffic system.

### C. Design of Cost Function and Constraints in DeeP-LCC

Motivated by DeePC (22), we show how to utilize the nonparametric behavior representation (29) to design the control input of the CAVs. We design the future behavior  $(u, \epsilon, y)$  for the mixed traffic system in a receding horizon manner. This is based on precollected data  $(u^d, \epsilon^d, \text{ and } y^d)$  and the most recent past data  $(u_{\text{ini}}, \epsilon_{\text{ini}}, \text{ and } y_{\text{ini}})$  that are updated online.

Compared to the standard DeePC (21), one unique feature of (29) is the introduction of the external input sequence, i.e., the velocity error  $\epsilon$  of the head vehicle. The past external input sequence  $\epsilon_{\text{ini}}$  can be collected in the control process, but the future external input sequence  $\epsilon$  cannot be designed and is also unknown in practice. Although its future behavior might be predicted based on traffic conditions ahead, it is nontrivial to achieve an accurate prediction. Since the driver always attempts to maintain the equilibrium velocity, one natural approach is to assume that the future velocity error of the head vehicle is zero, i.e.,

$$\epsilon = \mathbb{0}_N. \quad (30)$$

Similar to LCC [11], we consider the performance of the entire mixed traffic system in Fig. 1 for controller design. Precisely, we use a quadratic cost function  $J(y, u)$  to quantify the mixed traffic performance by penalizing the output deviation (recall that  $y$  in (8) represents the measurable deviation from equilibrium) and the energy of control input  $u$ , which is defined as

$$J(y, u) = \sum_{k=t}^{t+N-1} (\|y(k)\|_Q^2 + \|u(k)\|_R^2) \quad (31)$$

where the weight matrices  $Q$  and  $R$  are set as  $Q = \text{diag}(Q_v, Q_s)$  with  $Q_v = \text{diag}(w_v, \dots, w_v) \in \mathbb{R}^{n \times n}$ ,  $Q_s = \text{diag}(w_s, \dots, w_s) \in \mathbb{R}^{m \times m}$ , and  $R = \text{diag}(w_u, \dots, w_u) \in \mathbb{R}^{m \times m}$  with  $w_v, w_s$ , and  $w_u$  representing the penalty for the velocity errors of all the vehicles, spacing errors of all the CAVs, and control inputs of the CAVs, respectively.

Now, we introduce several constraints for CAV control in mixed traffic. First, the safety constraint for collision-free guarantees needs to be considered. To address this, we impose a lower bound on the spacing error of each CAV, which is given by

$$\tilde{s}_i \geq \tilde{s}_{\min}, \quad i \in S \quad (32)$$

with  $\tilde{s}_{\min}$  denoting the minimum spacing error for each CAV. With the appropriate choice of  $\tilde{s}_{\min}$ , the rear-end collision of the CAVs is avoided whenever feasible.



Second, to attenuate traffic perturbations, existing CAVs' controllers tend to leave an extremely large spacing from the preceding vehicle (see, e.g., [5] and the discussions in [13, Sec. V-D]), which in practice might cause vehicles from adjacent lanes to cut in. To tackle this problem, we introduce a maximum spacing constraint for each CAV, which is shown as follows:

$$\tilde{s}_i \leq \tilde{s}_{\max}, \quad i \in S \quad (33)$$

where  $\tilde{s}_{\max}$  represents the maximum spacing error. Recall that the spacing error of the CAVs is contained in the system output (8), whose future sequence  $y$  serves as a decision variable in behavior representation (29). Thus, we translate the constraints (32) and (33) on the spacing errors to the following constraint on future output sequence:

$$\tilde{s}_{\min} \leq I_N \otimes [\mathbf{0}_{m \times n} \quad I_m] y \leq \tilde{s}_{\max}. \quad (34)$$

Finally, the control input of each CAV is constrained considering the vehicular actuation limit, given as follows:

$$a_{\min} \leq u \leq a_{\max} \quad (35)$$

where  $a_{\min}$  and  $a_{\max}$  denote the minimum and the maximum acceleration, respectively.

#### D. Formulation of DeeP-LCC

We are now ready to present the following optimization problem to obtain the optimal control input of the CAVs:

$$\begin{aligned} \min_{g, u, y} \quad & J(y, u) \\ \text{s.t.} \quad & (29), (30), (34), (35). \end{aligned} \quad (36)$$

Note that unlike  $u$  and  $y$ , the future velocity error sequence  $\epsilon$  of the head vehicle, i.e., the external input of the mixed traffic system, is not a decision variable in (36); instead, it is fixed as a constant value, as shown in (30).

Furthermore, it is worth noting that the nonparametric behavior representation shown in Proposition 2 is valid for deterministic LTI mixed traffic systems. In practice, the car-following behavior of HDVs is nonlinear, as discussed in Section II-A, and also has certain uncertainties, leading to a nonlinear and nondeterministic mixed traffic system. Practical traffic data collected from such a nonlinear system are also noise-corrupted, and thus, the equality constraint (29) becomes inconsistent, i.e., the subspace spanned by the columns of the data Hankel matrices fails to coincide with the subspace of all valid trajectories of the underlying system.

Motivated by the regularized version of DeePC [26], we introduce a slack variable  $\sigma_y \in \mathbb{R}^{(n+m)T_{\text{ini}}}$  for the system past output to ensure the feasibility of the equality constraint and then solve the following regularized optimization problem:

$$\begin{aligned} \min_{g, u, y, \sigma_y} \quad & J(y, u) + \lambda_g \|g\|_2^2 + \lambda_y \|\sigma_y\|_2^2 \\ \text{s.t.} \quad & \begin{bmatrix} U_p \\ E_p \\ Y_p \\ U_f \\ E_f \\ Y_f \end{bmatrix} g = \begin{bmatrix} u_{\text{ini}} \\ \epsilon_{\text{ini}} \\ y_{\text{ini}} \\ u \\ \epsilon \\ y \end{bmatrix} + \begin{bmatrix} 0 \\ 0 \\ \sigma_y \\ 0 \\ 0 \\ 0 \end{bmatrix} \end{aligned} \quad (37)$$

(30), (34), (35).

#### Algorithm 2 DeeP-LCC for Mixed Traffic Control

---

**Input:** Pre-collected traffic data  $(u^d, \epsilon^d, y^d)$ , initial time  $t_0$ , terminal time  $t_f$ ;

- 1: Construct data Hankel matrices  $U_p, U_f, E_p, E_f, Y_p, Y_f$ ;
- 2: Initialize past traffic data  $(u_{\text{ini}}, \epsilon_{\text{ini}}, y_{\text{ini}})$  before the initial time  $t_0$ ;
- 3: **while**  $t_0 \leq t \leq t_f$  **do**
- 4:   Solve (37) for optimal predicted input  $u^* = \text{col}(u^*(t), u^*(t+1), \dots, u^*(t+N-1))$ ;
- 5:   Apply the input  $u(t) \leftarrow u^*(t)$  to the CAVs;
- 6:    $t \leftarrow t+1$  and update past traffic data  $(u_{\text{ini}}, \epsilon_{\text{ini}}, y_{\text{ini}})$ ;
- 7: **end while**

---

This formulation (37) is applicable to nonlinear and nondeterministic mixed traffic systems. In (37), the slack variable  $\sigma_y$  is penalized with a weighted two-norm penalty function, and the weight coefficient  $\lambda_y > 0$  can be chosen sufficiently large such that  $\sigma_y \neq 0$  only if the equality constraint is infeasible. In addition, a two-norm penalty on  $g$  with a weight coefficient  $\lambda_g > 0$  is also incorporated. Intuitively, the regularization term  $\lambda_g \|g\|_2^2$  reduces the “complexity” of the data-centric behavior representation and avoids overfitting, while the term  $\lambda_y \|\sigma_y\|_2^2$  improves the prediction accuracy while guaranteeing the representation feasibility. The introduction of the practical constraints (34) and (35) provides safety guarantees for the CAVs when they are feasible. The notion of recursive feasibility plays a critical role for safety guarantees. We refer the interested readers to a recent result [45, Proposition 1] on recursive feasibility of the standard DeePC under an upper level bounded condition on the slack variable  $\sigma_y$  and a terminal constraint of stabilizing the system at equilibrium within the predictive horizon  $N$ . Due to the page limit, we leave the recursive feasibility of DeeP-LCC for future work.

As shown in Fig. 1, our proposed DeeP-LCC mainly consists of two parts:

- 1) offline data collection, which records measurable input-output traffic data and constructs data Hankel matrices;
- 2) online predictive control, which relies on data-centric representation of system behavior for future trajectory prediction.

In particular, at each time step during online predictive control, we solve the final DeeP-LCC formulation (37) in a receding horizon manner. Algorithm 2 lists the procedure of DeeP-LCC. We note that problem (37) amounts to solve a quadratic program, for which very efficient and reliable solvers exist.

**Remark 3 (Regularization):** The regularization approach in (37) is common in the recent work on employing Willem's fundamental and DeePC for nonlinear and stochastic control [29], [31], [32], [33], [45], and [46]. From a theoretic perspective, it has been revealed in [29], [32] that the regulation on  $g$  coincides with distributional robustness. Some closed-loop properties, such as recursive feasibility and exponential stability, have also been rigorously proved in [45] and [46] for nonlinear and stochastic systems by imposing terminal constraints and typical auxiliary assumptions

(e.g., linear independence constraint qualification). In addition, the effectiveness of the regularization has been demonstrated in multiple empirical studies on practical nonlinear systems with noisy measurements, including quadcopter systems [31], power grids [32], and electric motor drives [33]. Motivated by the aforementioned research, we introduce this regularization into DeeP-LCC for the nonlinear and nondeterministic traffic systems. Note that unlike previous work [29], [32], [45], [46], our formulation (37) has an external disturbance input signal  $\epsilon$ , and we leave its theoretical investigation for future research. Indeed, it is observed from our nonlinear simulations in Section VI and our follow-up real-world miniature experiments in [47] that the proposed regularized formulation (37) achieves effective wave-dampening performance for CAVs in practical mixed traffic systems.  $\square$

*Remark 4 (External Input):* Compared to standard DeePC, we introduce the external input signal and utilize (30) to predict its future value. To address the unknown future external input, another approach is to assume a bounded future velocity error of the head vehicle. This idea is similar to robust DeePC against unknown external disturbances (see, e.g., [32], [48]). It is interesting to further design robust DeePC for mixed traffic when the head vehicle is oscillating around an equilibrium velocity, but this is beyond the scope of this work. In Section VI, our traffic simulations reveal that by assuming (30) and updating equilibrium based on historical velocity data of the head vehicle, the proposed DeeP-LCC has already shown excellent performance in improving traffic performance.  $\square$

*Remark 5 (Computational Complexity):* For mixed traffic control, both MPC and DeeP-LCC can be formulated into a quadratic program for numerical computation. In the DeeP-LCC formulation (37), one could use  $g \in \mathbb{R}^{T-T_{\text{ini}}-N+1}$  as the main decision variable, with an equality constraint given by  $U_p g = u_{\text{ini}} \in \mathbb{R}^{T_{\text{ini}}m}$  (here, the influence of the external input is neglected without loss of generality). As revealed in (27), the precollected data length  $T$  is lower bounded by  $(m+1)(T_{\text{ini}}+N+2n)-1$ , and thus, DeeP-LCC has at least  $2mn+2n+Nm$  free decision variables. For MPC, its optimization size is captured by the future control sequence  $u \in \mathbb{R}^{Nm}$ . Therefore, the online optimization size of DeeP-LCC is slightly larger than that of MPC with  $2mn+2n$  additional decision variables, but it is observed in Section VI that the computation time of DeeP-LCC is acceptable for small-scale simulations (about 28.07 ms). Meanwhile, the simplicity of DeeP-LCC is worth noting: it directly utilizes a single trajectory for online predictive control based on one integrated optimization formulation (37). In particular, it requires no prior knowledge of the system model and circumvents an offline model identification step and an online initial state estimation step, which are necessary steps in standard output-feedback MPC. Still, it is an important future direction to improve the computational efficiency of DeeP-LCC for large-scale mixed traffic flow. We refer the interested readers to [49] for a recent potential approach by distributed optimization.  $\square$

## VI. TRAFFIC SIMULATIONS

This section presents three nonlinear and nondeterministic traffic simulations to validate the performance of DeeP-LCC in mixed traffic. The nonlinear OVM model (2) is utilized to depict the dynamics of HDVs. A noise signal with the uniform distribution of  $\mathbb{U}[-0.1, 0.1]$  m/s<sup>2</sup> is added to acceleration dynamics model (2) of each HDV in our simulations.<sup>4</sup>

For the mixed traffic system in Fig. 1, we consider eight vehicles behind the head vehicle, among which there exist two CAVs and six HDVs, i.e.,  $n = 8$  and  $m = 2$  (this corresponds to a CAV penetration rate of 25%). The two CAVs are located at the third and the sixth vehicles, i.e.,  $S = \{3, 6\}$ . The parameter setup for DeeP-LCC is given as follows.

- 1) *Offline Data Collection:* The length for the precollected trajectory is chosen as  $T = 800$  with a sampling interval  $\Delta t = 0.05$  s. When collecting trajectories, we consider an equilibrium traffic velocity of 15 m/s, and the precollected datasets from this equilibrium are used for all the following experiments. For the system inputs, we utilize the OVM model (2) as a predesigned controller for the CAVs with random noise perturbations and assume a random slight perturbation on the head vehicle's velocity. Given a sufficiently long trajectory, this design naturally satisfies the persistent excitation requirement in Assumption 2 and is also applicable to practical traffic flow. More details and an illustration of a precollected trajectory can be found in Appendix B.
- 2) *Online Control Procedure:* The time horizons for the future signal sequence and past signal sequence are set to  $N = 50$  and  $T_{\text{ini}} = 20$ , respectively. In the cost function (31), the weight coefficients are set to  $w_v = 1$ ,  $w_s = 0.5$ , and  $w_u = 0.1$ ; for constraints, the boundaries for the spacing of the CAVs are set to  $s_{\text{max}} = 40$  m and  $s_{\text{min}} = 5$  m, and the limit for the acceleration of the CAVs is set to  $a_{\text{max}} = 2$  m/s<sup>2</sup> and  $a_{\text{min}} = -5$  m/s<sup>2</sup> (this limit also holds for all the HDVs via saturation). In the regulated formulation (37), the parameters are set to  $\lambda_g = 10$  and  $\lambda_y = 10000$ .

### A. Performance Validation Around an Equilibrium State

Motivated by [16], [22], and [35], our first experiment (Experiment A) simulates a traffic wave scenario, where vehicles accelerate and decelerate periodically, by imposing a sinusoidal perturbation on the head vehicle around the equilibrium velocity of 15 m/s (see the black profile in Fig. 3 for the velocity trajectory of the head vehicle), and investigates the performance of CAVs in dampening traffic waves. In particular, we aim to compare the performance of the proposed DeeP-LCC with the standard output-feedback MPC (23) based on an accurate mixed traffic system model (25). The dynamical model for all the HDVs is set to follow the nominal parameter values [6], [13], [16]:  $\alpha = 0.6$ ,  $\beta = 0.9$ ,  $v_{\text{max}} = 30$ ,  $s_{\text{st}} = 5$ ,  $s_{\text{go}} = 35$ , and  $v^* = 15$ . The MPC controller

<sup>4</sup>The algorithm and simulation scripts are available at <https://github.com/soc-ucsd/DeeP-LCC>

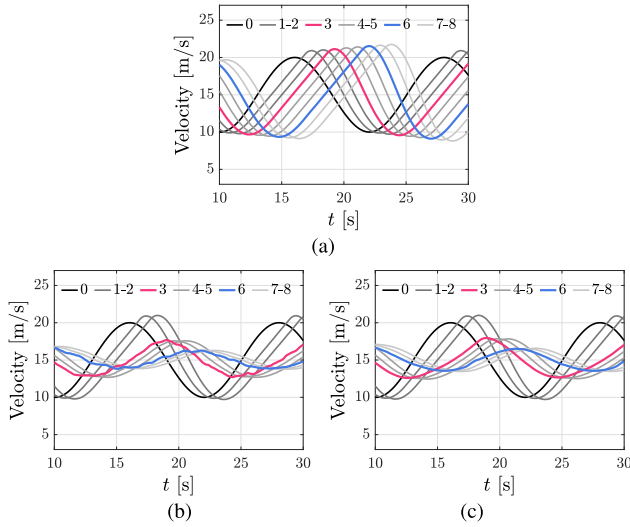


Fig. 3. Velocity profiles in Experiment A, where a sinusoidal perturbation is imposed on the head vehicle. The black profile represents the head vehicle (vehicle 0, and the gray profile represents the HDVs with different darkness denoting different vehicle indices. The red profile (vehicle 3) and the blue profile (vehicle 6) represent the first and the second CAV, respectively. (a) All the vehicles are HDVs. (b) CAVs utilize the MPC controller. (c) CAVs utilize the DeeP-LCC controller.

is designed using the accurate linearized model (25) around the same equilibrium velocity of 15 m/s as that in offline data collection, while DeeP-LCC is designed according to the procedures in Section V. The other parameters, e.g., the coefficients in cost function and past/future time horizon, remain the same between MPC and DeeP-LCC.

When all the vehicles are HDVs, it is observed in Fig. 3(a) that the amplitude of such perturbation is amplified along the propagation. This perturbation amplification greatly increases fuel consumption and collision risk in mixed traffic. In contrast, with two CAVs existing in traffic flow and employing either MPC or DeeP-LCC, the amplitude of the perturbation is clearly attenuated, as shown in Fig. 3(b) and (c), respectively. This demonstrates the capabilities of CAVs in dissipating undesired disturbances and stabilizing traffic flow using either MPC or DeeP-LCC.

We note that Fig. 3(c) shows the performance of DeeP-LCC using one single precollected trajectory. Different precollected trajectories might influence the performance of DeeP-LCC, as DeeP-LCC directly relies on these data to design the CAVs' control input. To see the influence, we collect 100 trajectories of the same length  $T = 800$  to construct the data Hankel matrices (37) and carry out the same experiment. Fig. 4 shows the cost value  $J$  given by (31) at each simulation under DeeP-LCC or MPC. Recall that MPC utilizes the accurate linearized dynamics for control input design, and its performance can be regarded as the optimal benchmark for the nonlinear traffic control around the equilibrium state. In comparison, DeeP-LCC directly relies on the raw trajectory data, and the regularization in (37) might influence the optimality of the original cost  $J(y, u)$ . From our random experiments, we observe that DeeP-LCC achieves a mean real cost that is quite close to the benchmark (losing only 4.8% optimality) for the noise-corrupted nonlinear traffic system without

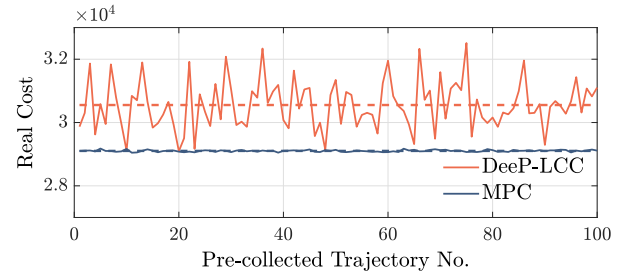


Fig. 4. Comparison of real cost between DeeP-LCC and MPC in 100 experiments in Experiment A. The dashed line represents the average real cost of each controller, which is  $2.91 \times 10^4$  for MPC and  $3.05 \times 10^4$  for DeeP-LCC with a standard deviation of  $0.003 \times 10^4$  and  $0.077 \times 10^4$ , respectively.

TABLE I  
HETEROGENEOUS PARAMETER SETUP FOR HDVs IN  
EXPERIMENTS B AND C

	$\alpha$	$\beta$	$s_{go}$
HDV 1	0.45	0.60	38
HDV 2	0.75	0.95	31
HDV 3	0.70	0.95	33
HDV 4	0.50	0.75	37
HDV 5	0.40	0.80	39
HDV 6	0.80	1.00	34
Nominal Setup	0.60	0.90	35

<sup>1</sup> The HDVs are indexed from front to end. For example, HDV 1 and HDV 2 are the two HDVs between the head vehicle and the first CAV.

<sup>2</sup> The other parameters follow the nominal setup:  $s_{st} = 5$ ,  $v_{max} = 30$ .

requiring any knowledge of the underlying system. These random experimental results validate the comparable wave-dampening performance of DeeP-LCC with respect to MPC based on accurate dynamics. This observation is consistent with previous studies of DeePC on other nonlinear dynamical systems such as quadcopters [26] or power grid [32].

### B. Traffic Improvement in Comprehensive Simulation

In Experiment A, we consider a fixed traffic equilibrium state and a nominal parameter setup for all HDVs. Here, in Experiment B, we design both an urban driving trajectory and a highway driving trajectory for the head vehicle motivated by ECE-15 and Extra-Urban Driving Cycle (EUDC) from the NEDC [50] and validate the capability of DeeP-LCC in improving traffic performance with time-varying equilibrium states. In addition, we assume a heterogeneous parameter setup around the nominal value for all the HDVs by utilizing the OVM model (2), see Table I. The MPC controller still utilizes the nominal parameter setup to design the control input, while DeeP-LCC relies on precollected trajectory data as usual. Note that practical traffic flow might have different equilibrium states in different time periods. In DeeP-LCC, we design a simple strategy to estimate equilibrium velocity by calculating the mean velocity of the head vehicle during the past horizon  $T_{ini}$  (the same time horizon for past signal sequence in DeeP-LCC). Meanwhile, the equilibrium spacing for the CAVs is chosen according to (13) using the OVM model with a nominal parameter setup (see Appendix C for more details).

To quantify traffic performance, we consider the fuel consumption and velocity errors for the vehicles indexed from

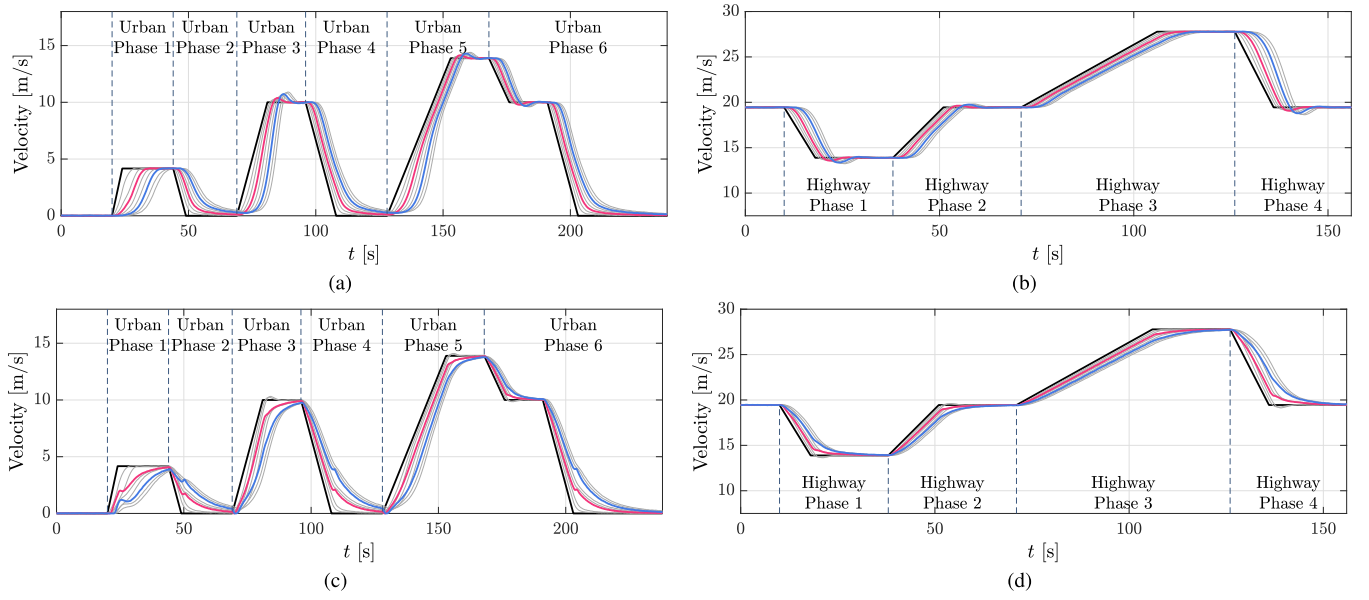


Fig. 5. Velocity profiles in Experiment B, which is designed, motivated by NEDC. (a) and (b) Case where all the vehicles are HDVs in the urban and highway scenarios, respectively. (c) and (d) Case where there are two CAVs utilizing DeeP-LCC in urban and highway scenarios. The color of each profile has the same meaning as that in Fig. 3.

3 to 8 since the first two HDVs cannot be influenced by the CAVs (recall that  $n = 8$  and  $S = \{3, 6\}$ ). Precisely, we utilize an instantaneous fuel consumption model in [51]: the fuel consumption rate  $f_i$  (mL/s) of the  $i$ th vehicle is calculated as

$$f_i = \begin{cases} 0.444 + 0.090 R_i v_i + [0.054 a_i^2 v_i]_{a_i > 0}, & \text{if } R_i > 0 \\ 0.444, & \text{if } R_i \leq 0 \end{cases}$$

where  $R_i = 0.333 + 0.00108 v_i^2 + 1.200 a_i$  with  $a_i$  denoting the acceleration of vehicle  $i$ . To quantify velocity errors, we use an index of mean squared velocity error (MSVE) given by

$$\text{MSVE} = \frac{\Delta t}{n(t_f - t_0)} \sum_{t=t_0}^{t_f} \sum_{i=1}^n (v_i(t) - v_0(t))^2$$

where  $t_0$  and  $t_f$  denote the begin time and end time of the simulation, respectively. This MSVE index depicts the tracking performance toward the velocity of the head vehicle and measures traffic smoothness.

The results of velocity trajectories of each vehicle are shown in Fig. 5. Compared to the case with all HDVs, DeeP-LCC allows the CAVs to rapidly track the trajectory of the head vehicle without overshoot and thus mitigates velocity perturbations and smooths the mixed traffic flow in both urban and highway scenarios. In addition, we observe that the improved traffic behavior under DeeP-LCC is close to that under MPC. By dividing the urban and highway driving cycles into different phases (see Fig. 5), we illustrate the reduction rate of fuel consumption and MSVE by MPC and DeeP-LCC with respect to the case with all HDVs in Fig. 6. Both MPC and DeeP-LCC contribute to a significant improvement in fuel economy and traffic smoothness. In particular, DeeP-LCC saves up to 9.05% fuel consumption during Phase 3 of urban driving scenarios and up to 43.82% velocity error during Phase 1 of highway driving scenarios.

Note that MPC utilizes the nominal model to design the control input, while DeeP-LCC relies on the trajectory data to directly predict the future system behavior. Thus, MPC is not easily applicable in practice since the nominal model for individual HDVs is generally unknown. In contrast, without explicitly identifying a parametric model, DeeP-LCC achieves a comparable performance with MPC using only precollected trajectory data, which are easier to acquire for the CAVs via V2V/V2I communications. In addition, although the optimization complexity of DeeP-LCC is slightly higher than that of MPC (see Remark 5), its mean computation time during this experiment is 28.07 ms in a laptop computer equipped with Intel Core i7-11800H CPU and 32-GB RAM. This computational cost is acceptable for real-time implementation in the underlying system scale (eight vehicles with two CAVs).

*Remark 6:* Previous work on validating CAVs' wave-dampening performance mostly considers a similar simulation scenario to Experiments A and C (sinusoidal or brake perturbation), see, e.g., [13], [16], [22], [35]. In our work, we have introduced the driving cycle, which is indeed mostly used for measuring fuel consumption and emission of one single vehicle, to further demonstrate the performance of DeeP-LCC in various traffic scenarios. In addition, note that in our data collection for DeeP-LCC, the traffic conditions around the fixed equilibrium velocity of 15 m/s are considered to capture the system behavior (see Appendix B for illustration of the precollected trajectory). In the simulations, however, the equilibrium is time-varying, and we assume that the HDVs have a similar behavior around different equilibrium states in order to make the fundamental lemma directly applicable with the data collected from one single equilibrium. This assumption indeed may not hold, and thus, the performance of DeeP-LCC might be compromised in this simulation. We provide further discussions and potential approaches to address time-varying equilibrium in Appendix C.  $\square$



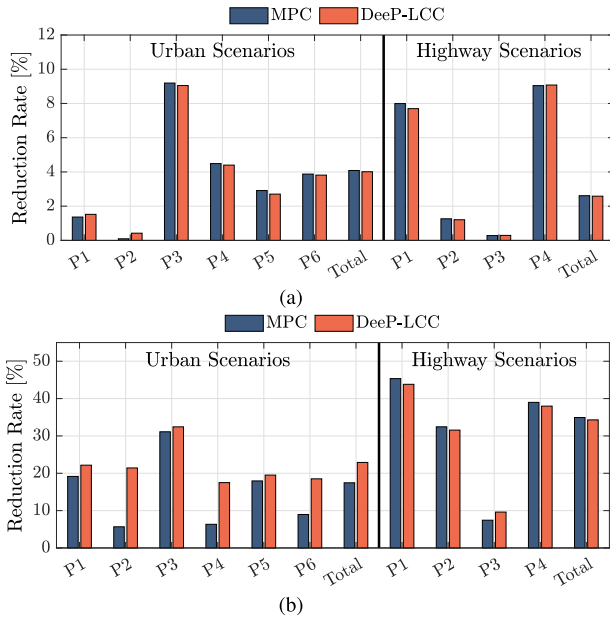


Fig. 6. Performance improvement of MPC and DeeP-LCC compared with the case where all the vehicles are HDVs in the comprehensive experiments. In the horizontal axis of each panel, P# is abbreviated for Phase #, denoting the phase number shown in Fig. 5. (a) Fuel consumption reduction rate. (b) MSVE reduction rate.

### C. Experiments in Emergence Braking Scenarios

To further validate the safety performance of DeeP-LCC, we design an emergence braking scenario motivated by Experiment B. As shown by the black profile in Fig. 7, the velocity of the head vehicle is: it maintains the normal velocity at the beginning; then, it takes a sudden emergency brake with the maximum deceleration and maintains the low velocity for a while; finally, it accelerates to the original normal velocity and maintains it in the rest time. This is a typical emergency case in real traffic, and it requires the CAVs' control to avoid rear-end collision. Note that the same precollected dataset around the equilibrium velocity of 15 m/s as the previous experiments is utilized in this simulation, and thus, as discussed in Section VI-B and Appendix C, the performance of DeeP-LCC could still be compromised.

The results are shown in Fig. 7. When all the vehicles are HDVs, they have a large velocity fluctuation in response to the brake perturbation of the head vehicle. In contrast, when two vehicles utilize DeeP-LCC, they have a different response pattern from the HDVs: the CAVs decelerate immediately when the head vehicle starts to brake, thus achieving a larger safe distance from the preceding vehicle [see the time period 0–10 s in Fig. 7(d)]; the CAVs also accelerate slowly when the head vehicle begins to return to the original velocity [see the time period 9–12 s in Fig. 7(f)]. In the case of all HDVs, they take a delayed rapid acceleration [see the time period 12–20 s in Fig. 7(e)], which lead to worse driving comfort and larger fuel consumption.

In addition, for this braking scenario, DeeP-LCC achieves a comparable performance with respect to MPC, which is designed based on prior linearized mixed traffic dynamics. Both strategies save a considerable rate of fuel consumption at

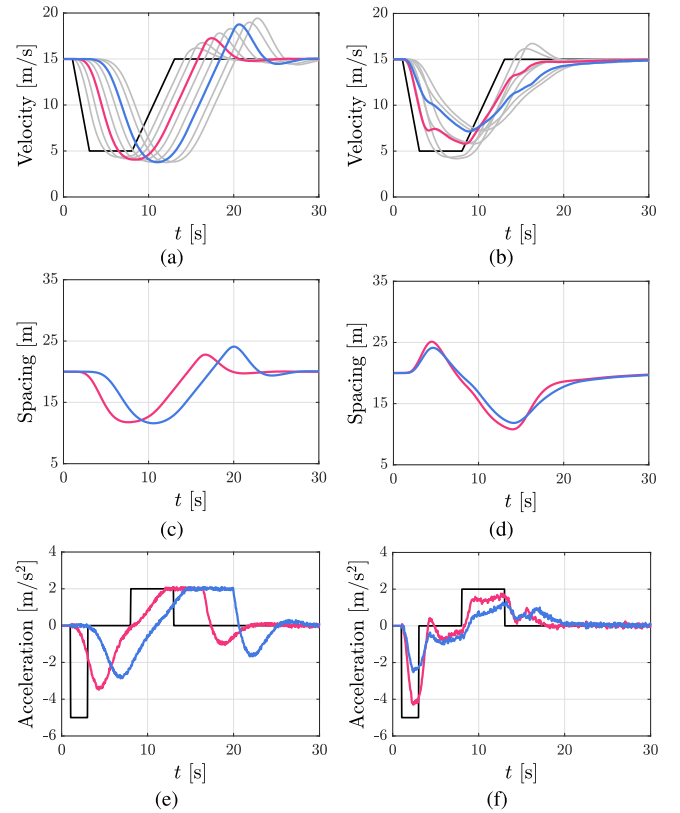


Fig. 7. Simulation results in Experiment C, where a sudden brake perturbation is imposed on the head vehicle. (a), (c), and (e) Velocity, spacing, and acceleration profiles, respectively, when all the vehicles are HDVs. (b), (d), and (f) Corresponding profiles where there are two CAVs utilizing the DeeP-LCC controller. In (c)–(f), the profiles of other HDVs are hidden. The color of each profile has the same meaning as that in Fig. 3.

a CAV penetration rate of 25% compared with the case of all HDVs (DeeP-LCC: 24.69% and MPC: 25.12%). This experiment result further demonstrates the capability of DeeP-LCC: it allows the CAVs to eliminate velocity overshoot, improve fuel economy, and constrain the spacing within the safe range while requiring no knowledge of HDVs' driving behaviors, contributing to more practical applications than MPC in real-world mixed traffic flow.

## VII. CONCLUSION

In this article, we have presented a novel DeeP-LCC for CAV control in mixed traffic with multiple HDVs and CAVs coexisting. Our dynamical modeling and controllability/observability analysis guarantees the rationality of the data-centric nonparametric representation of mixed traffic behavior in the linearized setup and further supports the feasibility of applying it to the nonlinear and stochastic mixed traffic system in real scenarios. In particular, DeeP-LCC directly relies on the trajectory data of the HDVs, bypassing a parametric HDV model, to design the CAVs' control input. Multiple numerical experiments confirm that DeeP-LCC achieves great improvement in traffic efficiency and fuel economy.

It is very interesting to adapt our current DeeP-LCC for time-varying traffic equilibrium states, in which we need to

investigate how to update precollected data for constructing Hankel matrices. To address system nonlinearity, besides introducing regularization and relaxation into the online optimization problem (37) in this article, it is also worth future investigations to establish a valid data-centric representation for mixed traffic dynamics with explicit consideration of nonlinear human driving behaviors. Communication delays are another important practical issue to consider in DeeP-LCC. Existing research has revealed the great potential of standard DeePC in addressing problems with delays [32]. In addition, the recursive feasibility of DeeP-LCC needs further investigation, which guarantees CAV control inputs within safety constraints. Finally, the computational efficiency of DeeP-LCC is worth further investigation for large-scale systems. Similar to distributed MPC [18] in CAV control, distributed versions of DeeP-LCC will also be extremely interesting.

## APPENDIXES

This appendix provides the proof of Theorem 1, detailed elaboration of offline data collection, and further discussions on the implementation of DeeP-LCC.

### A. Proof of Theorem 1

The following lemma is useful for proving Theorem 1.

**Lemma 4 (Controllability Invariance [41]):**  $(A, B)$  is controllable if and only if  $(A - BK, B)$  is controllable for any matrix  $K$  with compatible dimensions.

Based on Lemma 4, we transform system  $(A, B)$  in (15) into  $(\bar{A}, \bar{B})$  by introducing a virtual input  $\bar{u}(t)$ , which is defined as

$$\bar{u}(t) = [u_{i_1}(t), \bar{u}_{i_2}(t), \dots, \bar{u}_{i_m}(t)]^T \quad (38)$$

where for  $r = 2, \dots, m$ , we define

$$\bar{u}_{i_r}(t) = u_{i_r}(t) - (\alpha_1 \tilde{s}_{i_r}(t) - \alpha_2 \tilde{v}_{i_r}(t) + \alpha_3 \tilde{v}_{i_r-1}(t)).$$

Then, we have

$$\bar{u}(t) = u(t) - Kx(t) \quad (39)$$

where  $K = [0_n, \mathbb{e}_n^{i_2}, \dots, \mathbb{e}_n^{i_m}]^T \bar{K}$  and  $\bar{K}$  is given by

$$\bar{K} = \begin{bmatrix} 0 & & & & \\ k_{2,2} & k_{2,1} & & & \\ & \ddots & \ddots & & \\ & & k_{n,2} & k_{n,1} & \end{bmatrix} \in \mathbb{R}^{n \times 2n}$$

with

$$k_{i,1} = [\alpha_1 \quad -\alpha_2], \quad k_{i,2} = [0 \quad \alpha_3].$$

According to (39), we have  $A = \bar{A} - BK$ . By Lemma 4, controllability is consistent between  $(A, B)$  and  $(\bar{A}, \bar{B})$ . For system  $(\bar{A}, \bar{B})$ , the physical interpretation of the virtual input  $\bar{u}(t)$  in (38) is that except the control input of the first CAV, the control input signals of all the other CAVs contain a signal that follows the linearized car-following dynamics of HDVs (12).

Letting  $u_{i_r}(t) = 0$  ( $r = 2, \dots, m$ ), system  $(\bar{A}, \bar{B})$  is converted to a mixed traffic system with one single CAV—the only the CAV indexed as  $i_1$ , i.e., the first CAV in the mixed

traffic, has a control input. By Lemmas 1 and 2, which state the controllability of the mixed traffic system with one single CAV, system  $(\bar{A}, \bar{B})$  thus has the same controllability property. Since the controllability of  $(\bar{A}, \bar{B})$  and  $(A, B)$  is the same, we complete the proof of Theorem 1.

The proof of Corollary 1 is similar to that of Lemma 2 when  $S = \{1\}$ . We refer the interested readers to [11] for details.

### B. Offline Data Collection in DeeP-LCC

One critical issue in offline data collection of DeeP-LCC is to guarantee the persistent excitation requirement in Assumption 2 for the system input, consisting of CAVs' control inputs  $u(t)$  and the external input  $\epsilon(t)$ , i.e., velocity error of the head vehicle. To satisfy this assumption, we present the detailed discussions and the specific implementation method in our simulations as follows.

- 1) For the control input of the CAVs, in practice, we need a predesigned controller (e.g., a car-following model or an ACC-type controller) to control the motion of the CAVs in order to achieve CAV normal driving. Meanwhile, one could add certain i.i.d noise signal into the control model to enrich the control inputs. In our experiments, we utilize the OVM model (2) as a predesigned controller for the CAVs, and the control inputs are designed as

$$u_i(t) = \alpha(v_{\text{des}}(s_i(t)) - v_i(t)) + \beta \dot{s}_i(t) + \delta_u, \quad i \in S \quad (40)$$

where  $\delta_u \in [-1, 1]$  m/s<sup>2</sup>, and the parameters follow the nominal parameter setup in Table 1.

- 2) For the external input, it is known that in practice, the velocity of the head vehicle is under human control, and it is always oscillating slightly around the human driver's desired velocity. To simulate this scenario, we assume that the external input signal is given by

$$\epsilon(t) = \delta_\epsilon(k) \sim \mathcal{U}[-1, 1] \text{ m/s} \quad (41)$$

where  $t = 10k + b$  with  $k \in \mathbb{N}$ ,  $b \in \{0, 1, 2, \dots, 9\}$ , and  $\delta_\epsilon \sim \mathcal{U}[-1, 1]$  m/s. Recall that in the offline data collection for our experiments, we consider a fixed equilibrium velocity of 15 m/s, i.e., the head vehicle should have a mean velocity of 15 m/s. This design (41) means that its velocity changes randomly and slightly around the equilibrium velocity every ten time steps (0.5 s).

Due to the stochasticity of the input signals (40) and (41), the persistent excitation requirement can be satisfied when the input length is sufficiently long (since a longer trajectory leads to more columns in the Hankel matrix, making it easier to be full row rank). The theoretical lower bound on the input length  $T$  is  $(m+1)(T_{\text{ini}} + N + 2n) - 1$ , as revealed in (27), which is of value 257 in our experiments in Section VI, and we choose  $T = 800$  for redundancy considerations. One could verify the full rank condition by Definition 1 before applying the precollected dataset to controller design. We present one precollected trajectory in Fig. 8 for illustration, which is also utilized in Experiments B and C in Section VI.

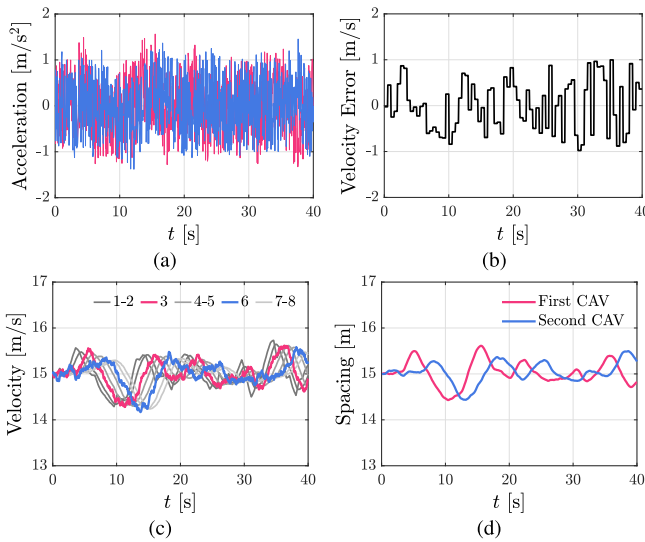


Fig. 8. Illustration of the precollected trajectory utilized in Experiments B and C. (a) and (b) System inputs, including the control input, i.e., the acceleration of the CAVs, and the external input, i.e., the velocity error of the head vehicle. (c) and (d) Measured system output, including the velocity of all the vehicles and the spacing of the CAVs.

### C. Practical Implementation With Time-Varying Equilibrium

In Section VI-A, we consider a fixed equilibrium state of 15 m/s for the simulated traffic flow. The trajectory data are collected around this state and the simulations are also carried out around it. In Sections VI-B and VI-C, we have utilized the average velocity of the head vehicle among the past horizon  $T_{ini}$  to estimate the equilibrium velocity. Precisely, at time  $t$ , we have

$$\begin{cases} v^* = \frac{1}{T_{ini}} \sum_{t-T_{ini}}^{t-1} v_0(t) \\ s^* = \arccos\left(1 - 2\frac{v^*}{v_{max}}\right) \cdot \frac{s_{go} - s_{st}}{\pi} + s_{st} \end{cases} \quad (42)$$

where the parameter values follow the nominal setup in Table I. This consideration enables the CAV to estimate the real-time equilibrium velocity and meanwhile have a human-like desired spacing policy, according to the OVM model (2). Combining this simple design (42) with DeeP-LCC, our simulation results have revealed the great potential of DeeP-LCC in improving traffic performance, although (42) might lead to mismatched equilibrium states.

When collecting trajectory data, we still consider the traffic flow around a fixed equilibrium velocity of 15 m/s to construct the data Hankel matrices. In DeeP-LCC, however, we obtain  $u_{ini}$  and  $y_{ini}$  by calculating the deviation from the time-varying equilibrium state obtained from (42). By assuming that the HDVs have a similar behavior around different equilibrium states, one could still apply the fundamental lemma to obtain valid control input.

This assumption does not always hold in practice, and thus, the performance demonstrated in the comprehensive simulation in Section VI-B and the braking simulation in Section VI-C might not fully reveal the potential of DeeP-LCC. In particular, there could be a mismatch between

the current mixed traffic behavior and the predicted behavior generated from the precollected datasets by Willems' fundamental lemma. To address this problem, one approach is to collect trajectory data from multiple equilibrium states, and when implementing DeeP-LCC, one can choose appropriate data (e.g., those data around the estimated current equilibrium state) to construct data Hankel matrices and design the control input. Another potential method is to update trajectory data utilized for data Hankel matrices by recording the real-time historical trajectory data in the control procedure. This method is also applicable to the case of time-varying mixed traffic behavior in order to capture the latest dynamics; see, e.g., [48] for applications in building control, where the new input-output measurements are appended on the right side of the Hankel matrices and the old data on the left side are discarded. Finally, it is also an interesting future direction to investigate the robustness performance of DeeP-LCC in mixed traffic in the case of behavior mismatch between data collection and real-time implementation.

### REFERENCES

- [1] G. Karagiannis et al., "Vehicular networking: A survey and tutorial on requirements, architectures, challenges, standards and solutions," *IEEE Commun. Surveys Tuts.*, vol. 13, no. 4, pp. 584–616, 4th Quart., 2011.
- [2] S. E. Li et al., "Dynamical modeling and distributed control of connected and automated vehicles: Challenges and opportunities," *IEEE Intell. Transp. Syst. Mag.*, vol. 9, no. 3, pp. 46–58, Jul. 2017.
- [3] Y. Zheng, S. Eben Li, J. Wang, D. Cao, and K. Li, "Stability and scalability of homogeneous vehicular platoon: Study on the influence of information flow topologies," *IEEE Trans. Intell. Transp. Syst.*, vol. 17, no. 1, pp. 14–26, Jan. 2016.
- [4] V. Milanés, S. E. Shladover, J. Spring, C. Nowakowski, H. Kawazoe, and M. Nakamura, "Cooperative adaptive cruise control in real traffic situations," *IEEE Trans. Intell. Transp. Syst.*, vol. 15, no. 1, pp. 296–305, Feb. 2014.
- [5] R. E. Stern et al., "Dissipation of stop-and-go waves via control of autonomous vehicles: Field experiments," *Transp. Res. C, Emerg. Technol.*, vol. 89, pp. 205–221, Apr. 2018.
- [6] Y. Zheng, J. Wang, and K. Li, "Smoothing traffic flow via control of autonomous vehicles," *IEEE Internet Things J.*, vol. 7, no. 5, pp. 3882–3896, May 2020.
- [7] K. Li, J. Wang, and Y. Zheng, "Cooperative formation of autonomous vehicles in mixed traffic flow: Beyond platooning," *IEEE Trans. Intell. Transp. Syst.*, vol. 23, no. 9, pp. 15951–15966, Sep. 2022.
- [8] S. E. Shladover, D. Su, and X.-Y. Lu, "Impacts of cooperative adaptive cruise control on freeway traffic flow," *Transp. Res. Rec., J. Transp. Res. Board*, vol. 2324, no. 1, pp. 63–70, Jan. 2012.
- [9] A. Talebpoor and H. S. Mahmassani, "Influence of connected and autonomous vehicles on traffic flow stability and throughput," *Transp. Res. C, Emerg. Technol.*, vol. 71, pp. 143–163, Oct. 2016.
- [10] G. Orosz, "Connected cruise control: Modelling, delay effects, and nonlinear behaviour," *Vehicle Syst. Dyn.*, vol. 54, no. 8, pp. 1147–1176, Aug. 2016.
- [11] J. Wang, Y. Zheng, C. Chen, Q. Xu, and K. Li, "Leading cruise control in mixed traffic flow: System modeling, controllability, and string stability," *IEEE Trans. Intell. Transp. Syst.*, vol. 23, no. 8, pp. 12861–12876, Aug. 2022.
- [12] E. Vinitsky, K. Parvate, A. Kreidieh, C. Wu, and A. Bayen, "Lagrangian control through deep-RL: Applications to bottleneck decongestion," in *Proc. 21st Int. Conf. Intell. Transp. Syst. (ITSC)*, Nov. 2018, pp. 759–765.
- [13] J. Wang, Y. Zheng, Q. Xu, J. Wang, and K. Li, "Controllability analysis and optimal control of mixed traffic flow with human-driven and autonomous vehicles," *IEEE Trans. Intell. Transp. Syst.*, vol. 22, no. 12, pp. 7445–7459, Dec. 2021.
- [14] C. Wu, A. R. Kreidieh, K. Parvate, E. Vinitsky, and A. M. Bayen, "Flow: A modular learning framework for mixed autonomy traffic," *IEEE Trans. Robot.*, vol. 38, no. 2, pp. 1270–1286, Apr. 2022.

- [15] Y. Sugiyama et al., "Traffic jams without bottlenecks—Experimental evidence for the physical mechanism of the formation of a jam," *New J. Phys.*, vol. 10, no. 3, Mar. 2008, Art. no. 033001.
- [16] J. I. Ge and G. Orosz, "Optimal control of connected vehicle systems with communication delay and driver reaction time," *IEEE Trans. Intell. Transp. Syst.*, vol. 18, no. 8, pp. 2056–2070, Aug. 2017.
- [17] Y. Zhou, S. Ahn, M. Wang, and S. Hoogendoorn, "Stabilizing mixed vehicular platoons with connected automated vehicles: An H-infinity approach," *Transp. Res. B, Methodol.*, vol. 132, pp. 152–170, Feb. 2020.
- [18] Y. Zheng, S. E. Li, K. Li, F. Borrelli, and J. K. Hedrick, "Distributed model predictive control for heterogeneous vehicle platoons under unidirectional topologies," *IEEE Trans. Control Syst. Technol.*, vol. 25, no. 3, pp. 899–910, May 2017.
- [19] B. Recht, "A tour of reinforcement learning: The view from continuous control," *Annu. Rev. Control, Robot., Auton. Syst.*, vol. 2, no. 1, pp. 253–279, 2019.
- [20] L. Furieri, Y. Zheng, and M. Kamgarpour, "Learning the globally optimal distributed LQ regulator," in *Proc. Learn. Dyn. Control*, 2020, pp. 287–297.
- [21] W. Gao, Z. Jiang, and K. Ozbay, "Data-driven adaptive optimal control of connected vehicles," *IEEE Trans. Intell. Transp. Syst.*, vol. 18, no. 5, pp. 1122–1133, May 2017.
- [22] M. Huang, Z. Jiang, and K. Ozbay, "Learning-based adaptive optimal control for connected vehicles in mixed traffic: Robustness to driver reaction time," *IEEE Trans. Cybern.*, vol. 52, no. 6, pp. 5267–5277, Jun. 2022.
- [23] E. F. Camacho and C. B. Alba, *Model Predictive Control*. Berlin, Germany: Springer, 2013.
- [24] J. Lan, D. Zhao, and D. Tian, "Data-driven robust predictive control for mixed vehicle platoons using noisy measurement," *IEEE Trans. Intell. Transp. Syst.*, vol. 24, no. 6, pp. 6586–6596, Jun. 2021.
- [25] L. Hewing, K. P. Wabersich, M. Menner, and M. N. Zeilinger, "Learning-based model predictive control: Toward safe learning in control," *Annu. Rev. Control, Robot., Auto. Syst.*, vol. 3, pp. 269–296, May 2020.
- [26] J. Coulson, J. Lygeros, and F. Dörfler, "Data-enabled predictive control: In the shallows of the DeepPC," in *Proc. 18th Eur. Control Conf. (ECC)*, 2019, pp. 307–312.
- [27] J. C. Willems, P. Rapisarda, I. Markovsky, and B. L. M. De Moor, "A note on persistency of excitation," *Syst. Control Lett.*, vol. 54, no. 4, pp. 325–329, Apr. 2005.
- [28] F. Fiedler and S. Lucia, "On the relationship between data-enabled predictive control and subspace predictive control," in *Proc. Eur. Control Conf. (ECC)*, Jun. 2021, pp. 222–229.
- [29] J. Coulson, J. Lygeros, and F. Dörfler, "Regularized and distributionally robust data-enabled predictive control," in *Proc. IEEE 58th Conf. Decis. Control (CDC)*, Dec. 2019, pp. 2696–2701.
- [30] F. Dörfler, J. Coulson, and I. Markovsky, "Bridging direct and indirect data-driven control formulations via regularizations and relaxations," *IEEE Trans. Autom. Control*, vol. 68, no. 2, pp. 883–897, Feb. 2023.
- [31] E. Elokda, J. Coulson, P. N. Beuchat, J. Lygeros, and F. Dörfler, "Data-enabled predictive control for quadcopters," *Int. J. Robust Nonlinear Control*, vol. 31, no. 18, pp. 8916–8936, Dec. 2021.
- [32] L. Huang, J. Coulson, J. Lygeros, and F. Dörfler, "Decentralized data-enabled predictive control for power system oscillation damping," *IEEE Trans. Control Syst. Technol.*, vol. 30, no. 3, pp. 1065–1077, May 2022.
- [33] P. G. Carlet, A. Favato, S. Bolognani, and F. Dörfler, "Data-driven predictive current control for synchronous motor drives," in *Proc. IEEE Energy Convers. Congr. Expo. (ECCE)*, Oct. 2020, pp. 5148–5154.
- [34] J. Wang, Y. Zheng, Q. Xu, and K. Li, "Data-driven predictive control for connected and autonomous vehicles in mixed traffic," in *Proc. Amer. Control Conf. (ACC)*, 2022, pp. 4739–4745.
- [35] M. Di Vaio, G. Fiengo, A. Petrillo, A. Salvi, S. Santini, and M. Tufo, "Cooperative shock waves mitigation in mixed traffic flow environment," *IEEE Trans. Intell. Transp. Syst.*, vol. 20, no. 12, pp. 4339–4353, Dec. 2019.
- [36] M. Bando, K. Hasebe, A. Nakayama, A. Shibata, and Y. Sugiyama, "Dynamical model of traffic congestion and numerical simulation," *Phys. Rev. E, Stat. Phys. Plasmas Fluids Relat. Interdiscip. Top.*, vol. 51, no. 2, pp. 1035–1042, Feb. 1995.
- [37] M. Treiber, A. Hennecke, and D. Helbing, "Congested traffic states in empirical observations and microscopic simulations," *Phys. Rev. E, Stat. Phys. Plasmas Fluids Relat. Interdiscip. Top.*, vol. 62, no. 2, pp. 1805–1824, Aug. 2000.
- [38] M. Treiber and A. Kesting, "Traffic flow dynamics," *Traffic Flow Dynamics: Data, Models and Simulation*. Berlin, Germany: Springer-Verlag, 2013.
- [39] G. Orosz, R. E. Wilson, and G. Stépán, "Traffic jams: Dynamics and control," *Phil. Trans. Roy. Soc. A: Math., Phys. Eng. Sci.*, vol. 368, no. 1928, pp. 4455–4479, Oct. 2010.
- [40] S. S. Mousavi, S. Bahrani, and A. Kouvelas, "Synthesis of output-feedback controllers for mixed traffic systems in presence of disturbances and uncertainties," *IEEE Trans. Intell. Transp. Syst.*, vol. 24, no. 6, pp. 6450–6462, Jun. 2022.
- [41] S. Skogestad and I. Postlethwaite, *Multivariable Feedback Control: Analysis and Design*, vol. 2. New York, NY, USA: Wiley, 2007.
- [42] L. Ljung, *System Identification*. New York, NY, USA: American Cancer Society, 2017.
- [43] I. Markovsky and P. Rapisarda, "Data-driven simulation and control," *Int. J. Control*, vol. 81, no. 12, pp. 1946–1959, Dec. 2008.
- [44] C.-T. Chen, *Linear System Theory and Design*. Philadelphia, PA, USA: Saunders College Publishing, 1984.
- [45] J. Berberich, J. Köhler, M. A. Müller, and F. Allgöwer, "Data-driven model predictive control with stability and robustness guarantees," *IEEE Trans. Autom. Control*, vol. 66, no. 4, pp. 1702–1717, Apr. 2021.
- [46] J. Berberich, J. Köhler, M. A. Müller, and F. Allgöwer, "Linear tracking MPC for nonlinear systems—Part II: The data-driven case," *IEEE Trans. Autom. Control*, vol. 67, no. 9, pp. 4406–4421, Sep. 2022.
- [47] J. Wang et al., "Implementation and experimental validation of data-driven predictive control for dissipating stop-and-go waves in mixed traffic," 2022, *arXiv:2204.03747*.
- [48] Y. Lian, J. Shi, M. Koch, and C. N. Jones, "Adaptive robust data-driven building control via bilevel reformulation: An experimental result," *IEEE Trans. Control Syst. Technol.*, early access, Mar. 30, 2023, doi: 10.1109/TCST.2023.3259641.
- [49] J. Wang, Y. Lian, Y. Jiang, Q. Xu, K. Li, and C. N. Jones, "Distributed data-driven predictive control for cooperatively smoothing mixed traffic flow," 2022, *arXiv:2210.13171*.
- [50] DieselNet. (2013). *Emission Test Cycles ECE 15 + EUDC/NEDC*. [Online]. Available: [https://dieselnet.com/standards/cycles/ece\\_eudc.php](https://dieselnet.com/standards/cycles/ece_eudc.php)
- [51] D. P. Bowyer, R. Akcelik, and D. Biggs, *Guide to Fuel Consumption Analyses for Urban Traffic Management*, no. 32. Melbourne, VIC, Australia: ARRB, 1985.



**Jiawei Wang** (Graduate Student Member, IEEE) received the B.E. degree in automotive engineering and the Ph.D. degree in mechanical engineering from Tsinghua University, Beijing, China, in 2018 and 2023, respectively.

During his Ph.D. research, he was a Visiting Ph.D. Student with the Automatic Control Laboratory, École Polytechnique (FC) d'École de Lausanne (EPFL), Lausanne, Switzerland, from 2021 to 2022. His research interests include connected automated vehicles, distributed control and optimization, and

data-driven control.

Dr. Wang was a recipient of the Outstanding Ph.D. Graduate, the Excellent Doctoral Dissertation Award, the National Scholarship, and the First-Class Scholarship at Tsinghua University. He received the Best Paper Award at the 18th COTA International Conference of Transportation Professionals in 2018 and the Annual Best Paper Award for the *Journal of Transport Information and Safety* in 2021.





**Yang Zheng** (Member, IEEE) received the B.E. and M.S. degrees from Tsinghua University, Beijing, China, in 2013 and 2015, respectively, and the D.Phil. (Ph.D.) degree in engineering science from the University of Oxford, Oxford, U.K., in 2019.

He was a Research Associate at Imperial College London, London, U.K., and a Post-Doctoral Scholar with Harvard John A. Paulson School of Engineering and Applied Sciences (SEAS) and Harvard Center for Green Buildings and Cities (CGBC), at Harvard University, Cambridge, MA, USA. He is currently an Assistant Professor with the Department of Electrical and Computer Engineering, University of California at San Diego, La Jolla, CA, USA. His research interests include learning, optimization, and control of network systems, and their applications to autonomous vehicles and traffic systems.

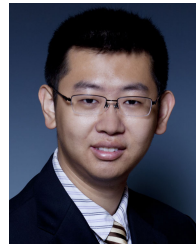
Dr. Zheng was a finalist (coauthor) for the Best Student Paper Award at the 2019 European Control Conference (ECC). He was a recipient of the Best Student Paper Award at the 17th IEEE Conference on Intelligent Transportation Systems in 2014, the Best Paper Award at the 14th Intelligent Transportation Systems Asia-Pacific Forum in 2015, the 2019 European Ph.D. Award on Control for Complex and Heterogeneous Systems, the 2022 Best Paper Award in the IEEE TRANSACTIONS ON CONTROL OF NETWORK SYSTEMS, the National Scholarship, the Outstanding Graduate at Tsinghua University, the Clarendon Scholarship at the University of Oxford, and the Chinese Government Award for Outstanding Self-financed Students Abroad.



**Keqiang Li** received the B.Tech. degree from Tsinghua University, Beijing, China, in 1985, and the M.S. and Ph.D. degrees in mechanical engineering from the Chongqing University of China, Chongqing, China, in 1988 and 1995, respectively.

He was the CTO of China ICV Research Institute Company Ltd. (CICV), Beijing. He is currently a Professor with the School of Vehicle and Mobility, Tsinghua University. He is leading the national key project on intelligent and connected vehicles (ICVs) in China. He has authored more than 200 articles and is a co-inventor of over 80 patents in China and Japan. His main research areas include automotive control systems, driver assistance systems, and networked dynamics and control.

Dr. Li served as a member for the Chinese Academy of Engineering, a fellow of the Society of Automotive Engineers of China, and the Chairperson for the Expert Committee of the China Industrial Technology Innovation Strategic Alliance for ICVs (CAICV). He was a recipient of the Changjiang Scholar Program Professor and the National Award for Technological Invention in China. He served on the Editorial Board of the *International Journal of Vehicle Autonomous Systems*.



**Qing Xu** received the B.S., M.S., and Ph.D. degrees in automotive engineering from Beihang University, Beijing, China, in 2006, 2008, and 2014, respectively.

During his Ph.D. research, he worked as a Visiting Scholar with the Department of Mechanical Science and Engineering, University of Illinois at Urbana-Champaign, Champaign, IL, USA. From 2014 to 2016, he had his post-doctoral research at Tsinghua University, Beijing, where he is currently working as an Associate Research Professor with the School of Vehicle and Mobility. His main research interests include the decision and control of intelligent vehicles.